Original Paper

nephron
Experimental
Nephrology

Nephron Exp Nephrol 2003;93:e117–e124
DOI: 10.1159/000069552

Received: July 5, 2002
Accepted: November 17, 2002

Caspase-9 Takes Part in Programmed Cell Death in Developing Mouse Kidney

Takashi Araki[a] Matsuhiko Hayashi[a] Keiko Nakanishi[b]
Nobuhiro Morishima[b] Takao Saruta[a]

[a]Department of Internal Medicine, Keio University School of Medicine, Tokyo; [b]Bioarchitect Research Group, Cellular and Molecular Biology Laboratory, RIKEN (Institute of Physical and Chemical Research), Saitama, Japan

Key Words
Caspase · Metanephros · Apoptosis · Nephrogenesis

Abstract
Programmed cell death is a mechanism by which organisms dispose of unwanted cells, and it is thought to be an important process in organogenesis. We have already reported the role of caspase-3 in the developing metanephros. While caspase-3 is thought to be positioned downstream of the caspase-activating cascade, the upstream caspase for programmed cell death in the developing kidney is still unknown. In an attempt to identify it, we blocked caspase activity in metanephric explants with caspase inhibitors. Administration of a caspase-9 inhibitor (Ac-IETD-CHO) effectively prevented both ureteric bud branching and nephrogenesis, the same as a caspase-3 inhibitor (Ac-DEVD-CHO). On the other hand, administration of a caspase-8 inhibitor (Ac-LETD-CHO) did not inhibit ureteric bud branching or nephrogenesis. Apaf-1, which executes programmed cell death in the caspase-9-related pathway, was detected in the cells exhibiting caspase-9 activity, and our results suggest that Apaaf-1/caspase-9 activates caspase-3 in kidney organogenesis.

Introduction

Apoptosis, or programmed cell death, is an essential physiological process that plays a critical role in controlling the number of cells in development by removing unwanted cells at the appropriate time [1]. About 50% of the cells are removed by programmed cell death during kidney development [2], and this is important for ureteric bud branching and tubule-like structure formation [3]. The caspase family cascade, series aspartate-specific cysteine proteases, appears to be the main pathway in executing programmed cell death. Since several members of the caspase family are processed by each other [4], resulting in effective amplification of cell death signals [4, 5], studies of the activation mechanisms of the apical caspases are crucial to understanding the cell death machinery. We have already reported the role of caspase-3 in the developing kidney [3]. Several caspase-activating pathways have recently been reported in executing programmed cell death. One is the DISC-forming apoptosis pathway, which includes Fas/Fas-L-inducing apoptosis and TNF/TNFR-inducing apoptosis [6–8], and caspase-8 is thought to activate caspase-3 in response to these stimuli. The other is mitochondrial apoptosis pathway, which includes changes in bcl-2 family proteins, for example bcl-2, bax, bid, and bik. Caspase-9 is important to this pathway [9], and caspase-9 and Apaf-1 complex are thought to activate caspase-3 in it [10, 11].

The cytosolic protein Apaf-1, which is the mammalian homolog of CED-4 of *Caenorhabditis elegans*, participates in the caspase-9-dependent activation of caspase-3

KARGER
Fax + 41 61 306 12 34
E-Mail karger@karger.ch
www.karger.com

1660–2129/03/0933–0117$19.50/0

Accessible online at:
www.karger.com/nee

Matsuhiko Hayashi, MD
Department of Internal Medicine, School of Medicine
Keio University, 35 Shinanomachi, Shinjuku-ku
Tokyo 160-8582 (Japan)
Tel. +81 3 5363 3796, Fax +81 3 3359 2745, E-Mail matsuhiko@sc.itc.keio.ac.jp

in the general apoptotic pathway [12, 13]. Apaf-1 plays a central role in the common events of mitochondria-dependent apoptosis in most death pathways, and its role is critical for normal development [14].

There are several pathways for executing programmed cell death, but the pathways whose participation is important to the programmed cell death of the developing kidney are unknown. To address this question, we blocked caspases in metanephric explants with a caspase-9 inhibitor and a caspase-8 inhibitor. Caspase-9 inhibition prevented both ureteric bud branching and tubule-like structure formation, which was similar to caspase-3 inhibition, but ureteric bud branching and tubule-like structure formation were not prevented by caspase-8 inhibition. Our results suggest that caspase-9 is an upstream caspase in kidney organogenesis and cell death in nondifferentiating mesenchyme.

Methods

Western Blotting Analysis for Caspase and Apoptosis-Related Gene Detection

Metanephroi of 12- and 16-dpc (days postcoitus; 12 and 16 days after mating) mouse embryos and kidneys of neonatal mice were collected, homogenized in 1 × SDS sample buffer, and boiled for 5 min. Protein samples were fractionated by electrophoresis in a 12.5% SDS-polyacrylamide gel and electrotransferred at 150 mA for 2 h. After blocking the membrane with 4% skim milk in PBST (0.2% Tween 20 in PBS) overnight at 4°C, it was incubated with anti-caspase-9 antibody (MBL, 1:200 dilution), anti caspase-8 antibody (Santa Cruz, 1:200 dilution, Calif., USA), anti-tubulin antibody (Calbiochem 1:500 dilution), and anti-Apaf-1 antibody (MBL, 1:200 dilution) overnight at 4°C, and then washed with PBST 3 times (for more than 5 min each time). The membrane was then incubated with HRP-conjugated anti-rabbit IgG (Amersham, 1:1,000 dilution) for 60 min at room temperature and washed with PBST 3 times. Finally, the membrane was incubated with an ECL kit (Amersham) for 1 min.

Kidney Organ Cultures

Kidney organ culture was performed as described previously [1, 15]. Embryos were dissected from 12-dpc ICR mice. Metanephroi and associated ureteric buds were microdissected en bloc and cultured on polycarbonate filter (pore size: 1.0 μm; Nuclepore) in serum-free Ham's F12:DMEM 1:1 (Invitrogen) medium with supplements as described elsewhere [16]. Caspase inhibitors (100 μ*M* of Ac-IETD-CHO for caspase-8, Ac-LETD-CHO for caspase-9, Ac-DEVD-CHO for caspase-3, and Ac-YVAD-CHO for caspase-1, Peptide Institute, Japan) were added. The medium was changed every 24 h, and after 72 h of culture, the metanephroi were measured and analyzed by immunohistochemistry and lectin staining.

Evaluation of Ureteric Bud Branching and Tubule Induction

To visualize ureteric bud growth, cultured whole metanephroi were fixed with cold methanol for 10 min, washed 3 times with PBST, and incubated in monoclonal anti-pancytokeratin (Sigma, 1:50 dilution) overnight at 4°C. Samples were washed with PBST 3 times and then incubated with Cy3-labeled anti-mouse IgG (Jackson Immuno Research, 1:50 dilution, Pa., USA). Samples were washed with PBST 3 times, mounted, and examined with a fluorescence microscope. To visualize tubule formation, fixed metanephroi were incubated with FITC-conjugated LT *(Lotus tetragonolobus)* lectin (Funakoshi, 1:50 dilution) for 180 min at room temperature. Samples were washed with PBST 3 times, mounted, and examined with a fluorescence microscope.

Detection of Apoptosis

Apoptotic cells in the cultured metanephroi were detected by a TUNEL method (DeadEnd Fluorometric TUNEL System; Promega). Cultured metanephroi were fixed in 4% PBS paraformaldehyde solution at room temperature for 4 h, soaked in 10% sucrose in PBS for 8 h and 30% sucrose in PBS for 8 h at 4°C, and finally embedded in OCT compound (TISSUE-TEK). Frozen samples were cut into 8-μm-thick sections. Sections were incubated with equilibration buffer for 10 min at room temperature and then at 37°C for 60 min with working-strength TdT reaction buffer. The reaction was stopped by 10 min incubation in 2 × SSC. After washed with PBS, the sections were incubated with Hoechst 33342 (10 μ*M*) to visualize the nuclei.

Immunohistochemical Detection of Active Caspase-9 and Apaf-1 in Metanephros

Immunohistochemical detection was performed to evaluate the relation between caspase-9 activity and Apaf-1 in developing kidney. After incubating 8-μm frozen sections of E16 metanephros with anti-Apaf-1 antibody (SANTA CRUZ, 1:100 dilution) at 4°C overnight, the slide was washed with PBS three times, then incubated with Rhodamine-conjugated donkey anti-goat antibody (1:200 dilution) for 2 h. It was then incubated with V1 antibody [17], (1:500 dilution) at 4°C overnight. Next, the slide was washed with PBS three times, and then incubated with FITC-conjugated donkey anti-rabbit IgG antibody (1:200 dilution) for 2 h and after washing with PBS 3 times, it was examined with a fluorescence microscope.

Statistical Analysis

Data are expressed as mean ± SD. Comparison between two groups was made using the unpaired t test. $p < 0.05$ was considered statistically significant.

Results

Expression of Caspases and Apaf-1 in Early Developing Kidneys

Western blotting was performed to examine the expression of caspase-8 and caspase-9, and both caspases were detected throughout embryonic kidney development (fig. 1). Expression of Apaf-1 was strongest in 12-dpc metanephroi, and decreased thereafter (fig. 1).

Caspase-9 Inhibitor Prevents Tubule-Like Product Formation in Developing Kidney

LT lectin is able to detect distal tubules in rat kidney [18] and tubule-like structures in developing kidney [1].

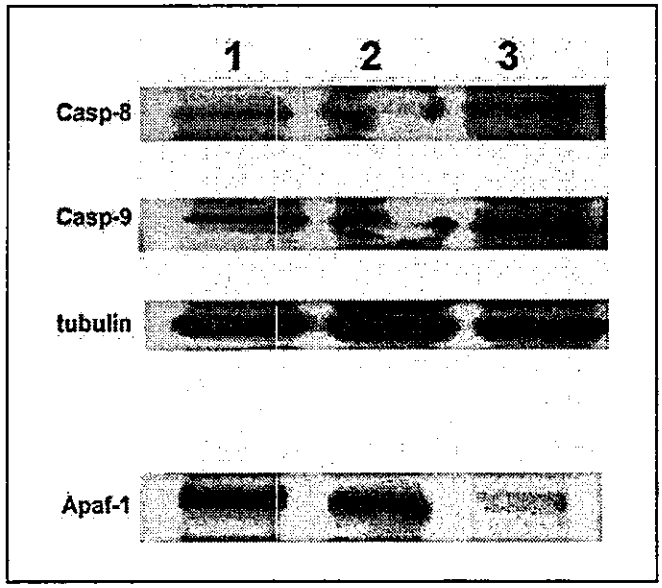

Fig. 1. Immunoblot analysis of caspase-8 and caspase-9 protein extracted from embryonic kidney. Lane 1 = Metanephroi of 12-dpc embryos; lane 2 = metanephroi of 16-dpc embryos; lane 3 = kidneys of neonatal mice.

LT lectin staining was performed to examine the effect of caspase inhibitors on the differentiation of mesenchymal cells into nephron-like structures. Neither caspase-1 inhibitor nor caspase-8 inhibitor affected the number of LT-lectin-positive structures in cultured metanephric explants (fig. 2, 3), whereas caspase-9 inhibitor decreased the number of LT-lectin-positive structures to 73.5% compared with the control (fig. 2, 3). Caspase-3 inhibitor also decreased the number of LT-lectin-positive structures to 60.1% (fig. 2, 3).

Caspase-9 Inhibitor Prevents Ureteric Bud Branching and Elongation in the Developing Kidney

To examine the effect of caspase inhibitors on the differentiation of mesenchymal cells, anti-pancytokeratin antibody, which detects the epithelial cells of proximal and distal tubules and of collecting ducts, was used in whole mount staining of cultured metanephroi with caspase inhibitors. When explants were cultured with the caspase-9 inhibitor Ac-IETD-CHO for 72 h, the number of branch points was reduced, and growth of the ureteric bud was suppressed, the same as with the caspase-3 inhibitor, Ac-DEVD-CHO. On the other hand, branching and elongation of the ureteric bud were not suppressed in explants cultured with the caspase-8 inhibitor, Ac-LETD-CHO, or the caspase-1 inhibitor, Ac-YVAD-CHO (fig. 4).

The Projected Surface Area of Metanephroi Was Restricted by Caspase-9 Inhibition

The ratio of the projected surface area of cultured metanephroi to 12-dpc metanephroi (percent) was indicated in figure 5. These ratios were not significantly changed by caspase-1 and caspase-8 inhibitors. However, the projected surface area of cultured metanephroi decreased when exposed to caspase-9 inhibitor, the same as when exposed to caspase-3 inhibitor (fig. 5).

Apoptosis in Cultured Metanephros was Inhibited by Caspase-9 Inhibition

Apoptotic cells were detected in non-differentiating mesenchymal cells around tubule-forming cells (fig. 6). With caspase-9 inhibition with Ac-IETD-CHO treatment, apoptotic cells in cultured metanephros decreased (fig. 6). Capase-8 inhibition with Ac-LETD-CHO and caspase-1 inhibition with Ac-YVAD-CHO did not affect the number of apoptotic cells in cultured metanephros (data not shown).

Caspase-9 Active Cells Expressed Apaf-1

To confirm the relation between Apaf-1 and caspase-9 activity, we performed immunohistochemical detection of Apaf-1 and caspase-9. Caspase-9 activity was determined by immunohistochemical detection of vimentin fragment, which was generated by caspase-9 [17]. While not all of the Apaf-1 positive cells was V1-positive, 90% of the V1-positive cells expressed Apaf-1 (fig. 7).

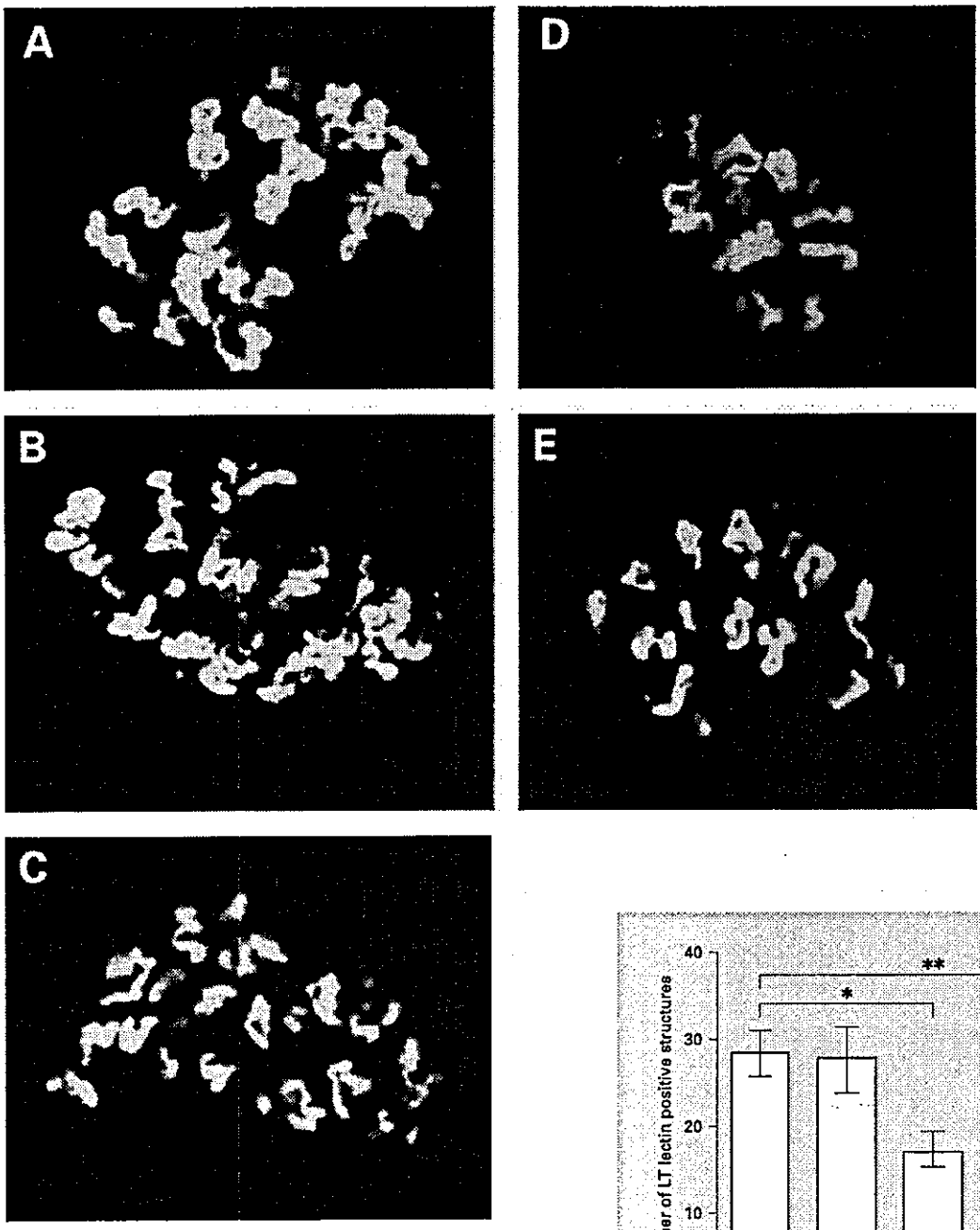

Fig. 2. Effect of caspase inhibitors on kidney development. LT-lectin staining was performed to evaluate nephrogenesis. **A** Control. **B** Ac-YVAD-CHO. **C** Ac-LETD-CHO. **D** Ac-DEVD-CHO. **E** Ac- IETD-CHO.

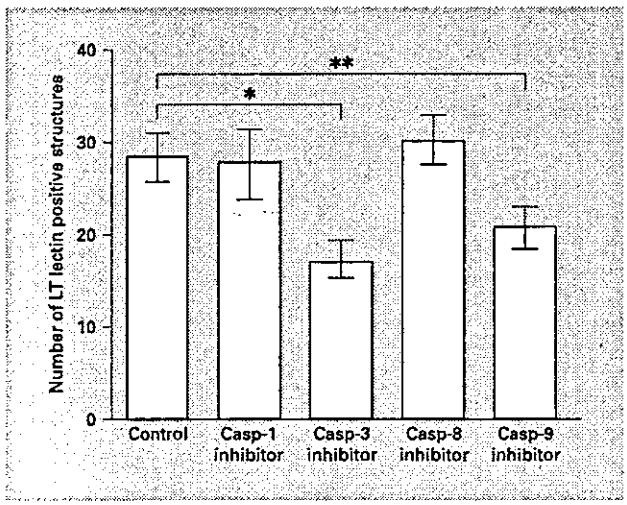

Fig. 3. Quantitative analysis of number of the LT-lectin positive structures. * $p < 0.01$ control vs. Ac-DEVD-CHO-treated metanephros; ** $p < 0.05$ control vs. Ac-IETD-CHO-treated metanephros, $n = 9$.

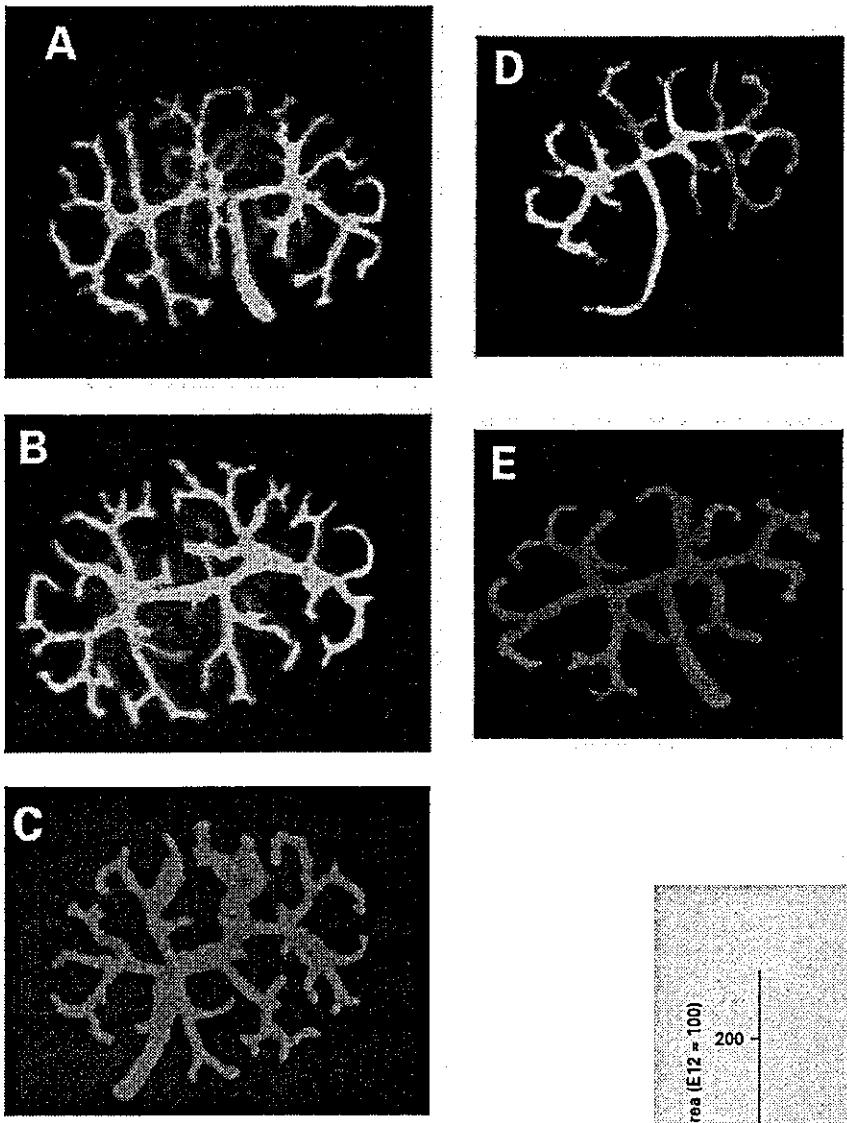

Fig. 4. Effect of caspase inhibitors on kidney development. Anti-pancytokeratin antibody staining of metanephros. Anti-pancytokeratin immunohistochemistry was performed to evaluate ureteric bud branching. **A** Control. **B** Ac-YVAD-CHO. **C** Ac-LETD-CHO. **D** Ac-DEVD-CHO. **E** Ac-IETD-CHO.

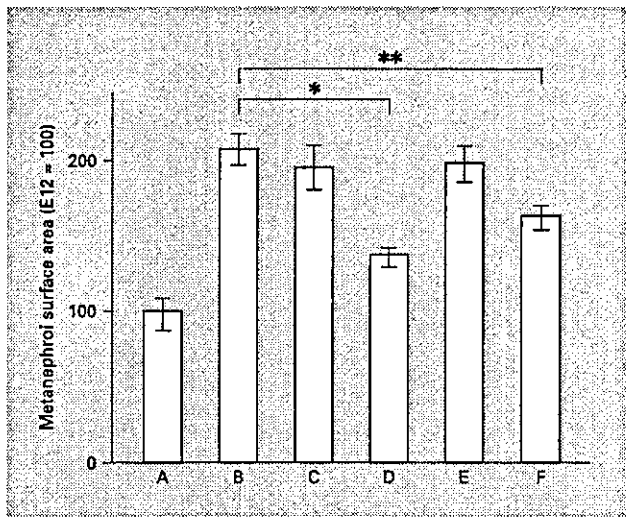

Fig. 5. The projected surface area of cultured metanephroi. **A** Metanephroi of 12-dpc embryos. **B** Control. **C** Ac-YVAD-CHO. **D** Ac-DEVD-CHO. **E** Ac-LETD-CHO. **F** Ac-IETD-CHO. * $p < 0.01$ control cultured metanephros versus Ac-DEVD-CHO-treated metanephros; ** $p < 0.05$ control cultured metanephros versus Ac-IETD-CHO-treated metanephros, $n = 9$.

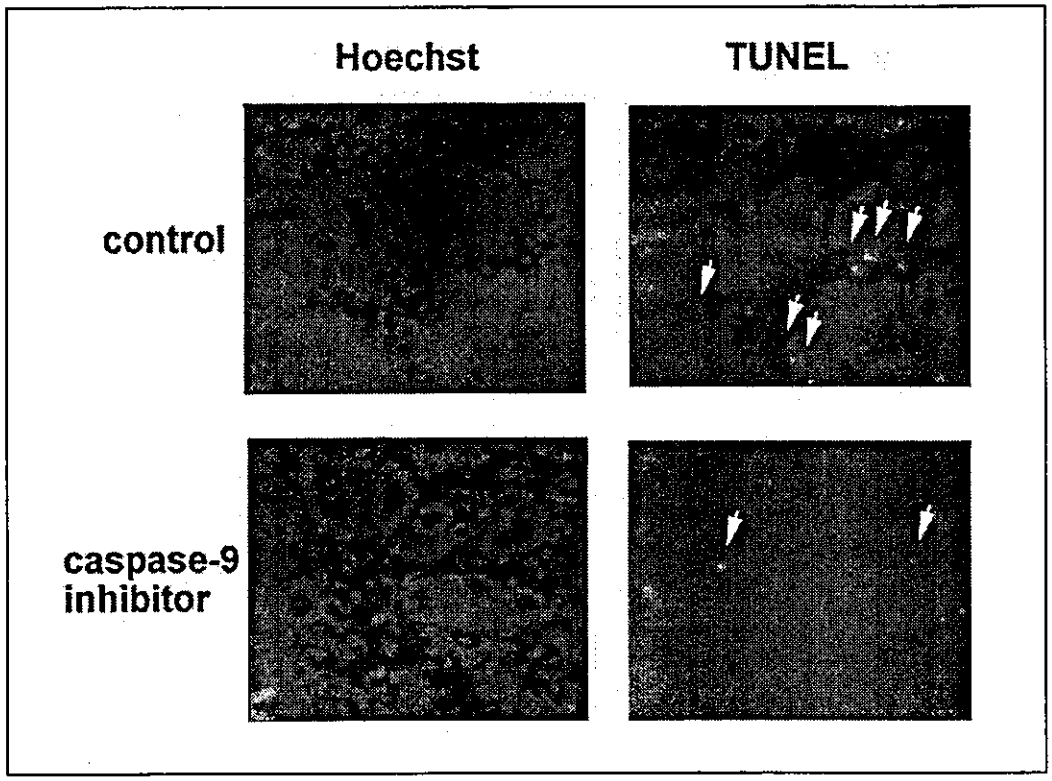

Fig. 6. Apoptotic cells in caspase-9 inhibitor-treated metanephros. TUNEL assay was performed for detecting apoptotic cells in cultured metanephros. Arrows indicate TUNEL-positive cells.

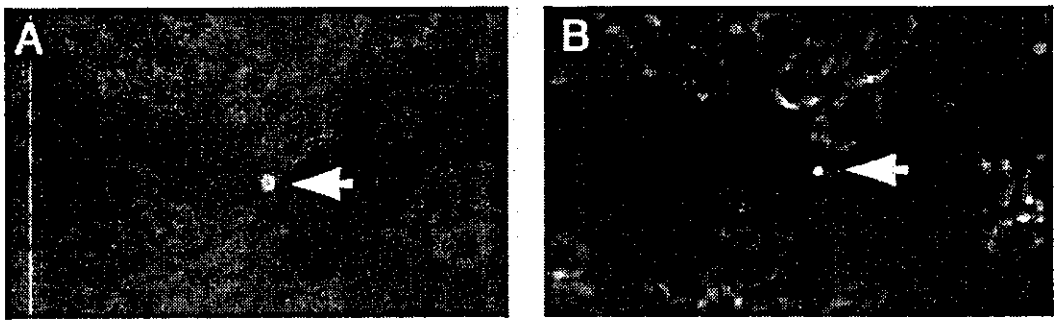

Fig. 7. Expression of Apaf-1 and caspase-9 activity in the developing kidney. **A** Apaf-1 staining. **B** Caspase-9 activity-positive cells.

Discussion

Programmed cell death plays an important role in organogenesis by controlling cell numbers in developing organs, and the execution of programmed cell death is conserved from *C. elegans* to mammals [19]. In *C. elegans*, CED-3 executes programmed cell death and CED-4 activates CED-3 [20–23], while in mammals, caspase-3, the mammalian homolog of CED-3, executes programmed cell death [24]. In mammals, inhibition of caspase activation results in disrupted neural tube closure [25]. In developing kidney, activation of caspase-3 appears to be a crucial event

in removing unwanted mesenchymal cells, and there are several pathways to activate caspase-3 in mammals. Caspase-8 and caspse-9 are well known to activate caspase-3 in mammalian cells [26, 27]. In the present study, we investigated how caspase-3 is activated in developing kidney.

The results of Western blot experiments showed that caspase-8 and caspase-9 are both expressed in developing kidney, and thus both were potential to activators of caspase-3 in developing kidney.

We performed organ culture of metanephros and blocked caspase activity by applying peptide caspase inhibitors. We had already performed organ culture with Z-D-CH_2DCB, a p35-like inhibitor of a broad spectrum of caspases [28], and found that it inhibited normal ureteric bud branching and differentiation to lectin-positive structures by inhibiting caspase-3 activation. Administration of caspase-9 inhibitor effectively prevented ureteric bud branching as shown by keratin immunohistochemistry. Nephron maturation was also inhibited by caspase-9 inhibitor, because the generation of LT-lectin-positive structures was decreased. Administration of caspase-8 inhibitor, however, did not inhibit ureteric bud branching or nephron maturation. In the previous paper, many of the apoptotic cells in developing kidney were observed in the cells surrounding the new epithelium [29]. The apoptotic cells were observed in the mesenchymal cells in organ cultured metanephros, but not in the nephron epithelial cells as the developing kidney. With caspase-9 inhibitor, the apoptotic cells of cultured metanephros decreased, and then the inhibiton of ureteric bud branching was suspected due to caspase-9 inhibition.

Apaf-1 works in the intrinsic pathway of caspase-3 activation together with caspase-9 and cytochrome C forming the apoptosome complex [30–32], which, in the presence of dATP, leads to activation of caspase-9 [30]. Active caspase-9, in turn, activates caspase-3. In the brain, RT-PCR experiments have revealed a marked decrease in Apaf-1 mRNA level in rat cortex after birth and maintenance at these levels in the mature brain [32]. We performed Western blot analysis and immunohistochemical analysis to clarify the contribution of Apaf-1 to programmed cell death in the developing kidney. Western blot analysis showed the strongest level of expression of Apaf-1 in E12 metanephros, with decreased expression during maturation, which is similar to brain development [33]. Caspase-9 activity was mainly detected in Apaf-1-positive cells. These observations suggest that caspase-9 and Apaf-1 works together in the developing kidney.

Activation of Drice is important to execute programmed cell death in the *Drosophila* apoptotic pathway [34]. Dronc, a CARD-containing CED-3/caspase-9 homolog, is activated by the CED-4/Apaf-1 homolog Hac-1, and activation of Dronc in turn activates Drice [35–37]. Programmed cell death is reduced in Hac-1 mutant drosophila embryos, and extra neurons are present. Activation of the death protease CED-3 is important to execute programmed cell death in the *C. elegans* apoptotic pathway, and the CED-3 mutants showed transformation of the fates of cells that normally die [38]. The activity of CED-3 appears to be controlled by CED-4 through a direct physical interaction [39]. Considering the apoptotic pathways of developing drosophila and *C. elegans* as a whole, Apaf-1 and caspase-9 may be important in controlling caspase-3 activation in the developmental stage of all species.

Antibody against the vimentin fragments generated by caspase-9 detects the peptide sequence recognized by caspase-9 [17], and Ac-IETD-CHO prevents IETD-cleaving activity, so it cannot be asserted that caspase-9 actually controls caspase-3 activation. However, IETD-cleaving enzymes, including caspase-9, may be crucial to kidney development.

We cannot exclude the possibility that other caspases activate caspase-3 in developing kidney, because the decrease in lectin-positive structures with caspase-9 inhibition was not as severe as caspase-3 inhibition. Caspase-8 may not be so important to the programmed cell death in developing kidney, but the possibility of participation of other pathways to activate caspase-3 cannot be ruled out by our methods.

Histological abnormalities are not observed in the kidneys of Apaf-1 –/– mice, which show histological abnormalities in neurological systems [12]. However, the genes related to programmed cell death belong to several families of protein, for example, KIAP is an IAP family protein, which is mainly expressed in fetal kidney [40], and thus there is a possibility that Apaf-1 has a kidney-specific family protein.

In conclusion, caspase-9 activity regulates caspase-3 activation in a part in developing kidney as well as organogenesis of the developing kidney, especially in ureteric bud branching and tubule-like structure formation, and Apaf-1 may be required for caspase-9 activation in developing kidney.

Acknowledgement

This research was supported in part by grants from the Ministry of Education, Science and Culture in Japan and from the Naito Foundation to *T.A*, and from Health Science Research Grants from the Ministry of Health and Welfare to *M.H.*

References

1 Jacobson MD, Weil M, Raff MC: Programmed cell death in animal development. Cell 1997; 88:347–354.
2 Coles HS, Burne JF, Raff MC: Large-scale normal cell death in the developing rat kidney and its reduction by epidermal growth factor. Development 1993;118:777–784.
3 Araki T, Saruta T, Okano H, Miura M: Caspase activity is required for nephrogenesis in the developing mouse metanephros. Exp Cell Res 1999;248:423–429.
4 Thornberry NA, Rano TA, Peterson EP, Rasper DM, Timkey T, Garcia-Calvo M, Houtzager VM, Nordstrom PA, Roy S, Vaillancourt JP, Chapman KT, Nicholson DW: A combinatorial approach defines specificities of members of the caspase family and granzyme B: Functional relationships established for key mediators of apoptosis. J Biol Chem 1997;272: 17907–17911.
5 Enari M, Talanian RV, Wong WW, Nagata S: Sequential activation of ICE-like and CPP32-like proteases during Fas-mediated apoptosis. Nature 1996;380:723–726.
6 Ashkenazi A, Dixit VM: Death receptors: Signaling and modulation. Science 1998;281: 1305–1308.
7 Kischkel FC, Hellbardt S, Behrmann I, Germer M, Pawlita M, Krammer PH, Peter ME: Cytotoxicity-dependent APO-1 (Fas/CD95)-associated proteins form a death-inducing signaling complex (DISC) with the receptor. EMBO J 1995;14:5579–5588.
8 Weber CH, Vincenz C: A docking model of key components of the DISC complex: Death domain superfamily interactions redefined. FEBS Lett 2001;492:171–176.
9 Costantini P, Bruey JM, Castedo M, Metivier D, Loeffler M, Susin SA, Ravagnan L, Zamzami N, Garrido C, Kroemer G: Pre-processed caspase-9 contained in mitochondria participates in apoptosis. Cell Death Differ 2002;9: 82–88.
10 Yang X, Chang HY, Baltimore D: Essential role of CED-4 oligomerization in CED-3 activation and apoptosis. Science 1998;281:1355–1357.
11 Cheng EH, Wei MC, Weiler S, Flavell RA, Mak TW, Lindsten T, Korsmeyer SJ: BCL-2, BCL-X(L) sequester BH3 domain-only molecules preventing BAX- and BAK-mediated mitochondrial apoptosis. Mol Cell 2001;8:705–711.
12 Cecconi F, Alvarez BG, Meyer BI, Roth KA, Gruss P: Apaf1 (CED-4 homolog) regulates programmed cell death in mammalian development. Cell 1998;94:727–737.
13 Teitz T, Wei T, Liu D, Valentine V, Valentine M, Grenet J, Lahti JM, Kidd VJ: Caspase-9 and Apaf-1 are expressed and functionally active in human neuroblastoma tumor cell lines with 1p36 LOH and amplified MYCN. Oncogene 2002;21:1848–1858.
14 Yoshida H, Kong YY, Yoshida R, Elia AJ, Hakem A, Hakem R, Penninger JM, Mak TW: Apaf1 is required for mitochondrial pathways of apoptosis and brain development. Cell 1998; 94:739–750.
15 Saxen L, Lehtonen E: Embryonic kidney in organ culture. Differentiation 1987;36:2–11.
16 Perantoni AO, Dove LF, Williams CL: Induction of tubules in rat metanephrogenic mesenchyme in the absence of an inductive tissue. Differentiation 1991;48:25–31.
17 Nakanishi K, Maruyama M, Shibata T, Morishima N: Identification of a caspase-9 substrate and detection of its cleavage in programmed cell death during mouse development. J Biol Chem 2001;276:41237–41244.
18 Elliget KA, Trump BF: Primary cultures of normal rat kidney proximal tubule epithelial cells for studies of renal cell injury. In Vitro Cell Dev Biol 1991;27A:739–748.
19 Meier P, Finch A, Evan G: Apoptosis in development. Nature 2000;407:796–801.
20 Yuan JY, Horvitz HR: The *Caenorhabditis elegans* genes ced-3 and ced-4 act cell autonomously to cause programmed cell death. Dev Biol 1990;138:33–41.
21 Hengartner MO, Horvitz HR: Programmed cell death in *Caenorhabditis elegans*. Curr Opin Genet Dev 1994;4:581–586.
22 Seshagiri S, Miller LK: *Caenorhabditis elegans* CED-4 stimulates CED-3 processing and CED-3-induced apoptosis. Curr Biol 1997;7:455–460.
23 Chinnaiyan AM, Chaudhary D, O'Rourke K, Koonin EV, Dixit VM: Role of CED-4 in the activation of CED-3. Nature 1997;388:728–729.
24 Fernandes-Alnemri T, Litwack G, Alnemri ES: CPP32, a novel human apoptotic protein with homology to *Caenorhabditis elegans* cell death protein Ced-3 and mammalian interleukin-1 beta-converting enzyme. J Biol Chem 1994; 269:30761–30764.
25 Weil M, Jacobson MD, Raff MC: Is programmed cell death required for neural tube closure? Curr Biol 1997;7:281–284.
26 Fernandes-Alnemri T, Armstrong RC, Krebs J, Srinivasula SM, Wang L, Bullrich F, Fritz LC, Trapani JA, Tomaselli KJ, Litwack G, Alnemri ES: In vitro activation of CPP32 and Mch3 by Mch4, a novel human apoptotic cysteine protease containing two FADD-like domains. Proc Natl Acad Sci USA 1996;93:7464–7469.
27 Kuida K, Haydar TF, Kuan CY, Gu Y, Taya C, Karasuyama H, Su MS, Rakic P, Flavell RA: Reduced apoptosis and cytochrome c-mediated caspase activation in mice lacking caspase 9. Cell 1998;94:325–337.
28 Hisahara S, Shoji S, Okano H, Miura M: ICE/CED-3 family executes oligodendrocyte apoptosis by tumor necrosis factor. J Neurochem 1997;69(1):10–20.
29 Koseki C, Herzlinger D, al-Awqati Q: Apoptosis in metanephric development. J Cell Biol 1992;119:1327–1333.
30 Li P, Nijhawan D, Budihardjo I, Srinivasula SM, Ahmad M, Alnemri ES, Wang X: Cytochrome c and dATP-dependent formation of Apaf-1/caspase-9 complex initiates an apoptotic protease cascade. Cell 1997;91(4):479–489.
31 Zou H, Henzel WJ, Liu X, Lutschg A, Wang X: Apaf-1, a human protein homologous to *C. elegans* CED-4, participates in cytochrome C-dependent activation of caspase-3. Cell 1997; 90(3):405–413.
32 Zou H, Li Y, Liu X, Wang X: An APAF-1 cytochrome C multimeric complex is a functional apoptosome that activates procaspase-9. J Biol Chem 1999;274(17):11549–11556.
33 Yakovlev AG, Ota K, Wang G, Movsesyan V, Bao WL, Yoshihara K, Faden AI: Differential expression of apoptotic protease-activating factor-1 and caspase-3 genes and susceptibility to apoptosis during brain development and after traumatic brain injury. J Neurosci 2001;21: 7439–7446.
34 Fraser AG, McCarthy NJ, Evan GI: drICE is an essential caspase required for apoptotic activity in *Drosophila* cells. EMBO J 1997;16: 6192–6199.
35 Hawkins CJ, Yoo SJ, Peterson EP, Wang SL, Vernooy SY, Hay BA: The *Drosophila* caspase DRONC cleaves following glutamate or aspartate and is regulated by DIAP1, HID, and GRIM. J Biol Chem 2000;275:27084–27093.
36 Kanuka H, Sawamoto K, Inohara N, Matsuno K, Okano H, Miura M: Control of the cell death pathway by Dapaf-1, a *Drosophila* Apaf-1/CED-4-related caspase activator. Mol Cell 1999;4:757–769.
37 Zhou L, Song Z, Tittel J, Steller H: HAC-1, a *Drosophila* homolog of APAF-1 and CED-4 functions in developmental and radiation-induced apoptosis. Mol Cell 1999;4:745–755.
38 Ellis HM, Horvitz HR: Genetic control of programmed cell death in the nematode C. elegans. Cell 1986;44:817–829.
39 Irmler M, Hofmann K, Vaux D, Tschopp J: Direct physical interaction between the *Caenorhabditis elegans* 'death proteins' CED-3 and CED-4. FEBS Lett 1997;406:189–190.
40 Lin JH, Deng G, Huang Q, Morser J: KIAP, a novel member of the inhibitor of apoptosis protein family. Biochem Biophys Res Commun 2000;279:820–831.

Disease-causing mutant WNK4 increases paracellular chloride permeability and phosphorylates claudins

Kozue Yamauchi, Tatemitsu Rai, Katsuki Kobayashi, Eisei Sohara, Tatsunori Suzuki, Tomohiro Itoh, Shin Suda, Atsushi Hayama, Sei Sasaki, and Shinichi Uchida*

Department of Nephrology, Graduate School, Tokyo Medical and Dental University, 1-5-45 Yushima Bunkyo, Tokyo 113-8519, Japan

Edited by Maurice B. Burg, National Institutes of Health, Bethesda, MD, and approved January 28, 2004 (received for review October 26, 2003)

Mutations in the WNK4 gene cause pseudohypoaldosteronism type II (PHAII), an autosomal-dominant disorder of hyperkalemia and hypertension. The target molecules of this putative kinase and the molecular mechanisms by which the mutations cause the phenotypes are currently unknown. Although recent reports found that expression of WNK4 in *Xenopus* oocytes causes inhibition of the thiazide-sensitive NaCl cotransporter and the renal K channel ROMK, there may be additional targets of WNK4. For example, an increase in paracellular chloride permeability has been postulated to be a mediator of PHAII pathogenesis, a possibility supported by the localization of WNK4 at tight junctions *in vivo*. To determine the validity of this hypothesis, we measured transepithelial Na and Cl permeability in Madin–Darby canine kidney II cells stably expressing wild-type or a pathogenic mutant of WNK4. We found that transepithelial paracellular Cl permeability was increased in cells expressing a disease-causing mutant WNK4 (D564A) but that Na permeability was decreased slightly. Furthermore, WNK4 bound and phosphorylated claudins 1–4, major tight-junction membrane proteins known to be involved in the regulation of paracellular ion permeability. The increases in phosphorylation of claudins were greater in cells expressing the mutant WNK4 than in cells expressing wild-type protein. These results clearly indicate that the pathogenic WNK4 mutant possesses a gain-of-function activity and that the claudins may be important molecular targets of WNK4 kinase. The increased paracellular "chloride shunt" caused by the mutant WNK4 could be the pathogenic mechanism of PHAII.

Pseudohypoaldosteronism type II (PHAII) [OMIM (online Mendelian inheritance in man) database no. 145260] is a rare Mendelian form of hypertension. Recently, mutations in two homologous protein kinase genes, *WNK1* and *WNK4*, were linked to PHAII by positional cloning (1). Determination of the pathogenesis of rare Mendelian forms of high blood pressure may provide important clues to the pathways underlying more common hypertension, termed "essential" hypertension, and may help identify new therapeutic targets. PHAII-causing mutations in the *WNK1* gene are large deletions in the first intron that appear to increase WNK1 expression. On the other hand, mutations in the *WNK4* gene are missense mutations that cluster within a span of four amino acids distal to the first putative coil domain (1). However, the consequence of these missense mutations for WNK4 function is poorly understood.

WNK1 and WNK4 are expressed in the distal nephron, suggesting that both kinases are involved in a previously unrecognized signaling pathway that regulates NaCl resorption in the distal nephron. However, the upstream regulators and the downstream molecular targets of these kinases are currently unknown. Based on clinical observations, two hypotheses have been proposed to explain the pathogenesis of PHAII. First, the mutations may cause an increase in distal nephron chloride permeability, also known as a "chloride shunt" (2). This increased chloride permeability would increase Na resorption and depolarize the transepithelial voltage, leading to hypertension and hyperkalemia, respectively. The second possibility is that the mutations increase the activity of the Na-dependent Cl cotransporter (TSC). This possibility is supported by the fact that PHAII can be treated with thiazide diuretics (3).

Recently, inhibition of TSC activity by wild-type WNK4, but not by the disease-causing mutant, was demonstrated in *Xenopus* oocytes (4, 5). Very recently, inhibition of the surface expression of ROMK channel by wild-type WNK4 was also reported. Interestingly, the disease-causing mutant further inhibited the surface expression of ROMK (6). However, these functional assays were performed only in *Xenopus* oocytes, and, to our knowledge, there have not been reports on the substrates of WNK4. TSC and ROMK are localized in the apical plasma membranes of distal nephron segments (7–9), whereas WNK4 is present in the tight-junction complexes in the cortical collecting ducts as well as in DCT (1). This finding suggests that there may be other molecular targets of WNK4, possibly including tight-junction proteins.

In this study, we first examined whether the expression of the wild-type or the disease-causing mutant WNK4 affects transepithelial paracellular ion permeability. To this end, we generated stable Madin–Darby canine kidney II (MDCK II) cell lines expressing the wild-type and one of the human disease-causing mutants (D564A) of WNK4 by using a tetracycline-inducible system. We found that transepithelial paracellular Cl permeability was increased in cells expressing the mutant WNK4. Accordingly, we searched for the downstream molecular target of WNK4 in tight-junction proteins.

Materials and Methods

Generation of WNK4-Expressing Cell Lines. Human WNK4 cDNA was isolated by RT-PCR using human kidney mRNA as a template. The cDNA was cloned into the pTRE2-hyg vector (Clontech) and a C-terminal hemagglutinin (HA) tag was added. We also generated a WNK4 construct with an N-terminal Flag-tag. The disease-causing mutation (D564A) was introduced with the QuikChange site-directed mutagenesis kit (Stratagene). Stable cell lines were isolated by using Tet-off MDCK II cells (Clontech) as a host cell line with selection by using hygromycin B (200 μg/ml). Cell lines were screened by immunoblotting. Rat anti-HA mAb (9Y10) (Roche Diagnostics) and mouse M2 mAb or rabbit anti-Flag Ab (Sigma) were used to detect HA-tagged and Flag-tagged proteins, respectively. Endogenous claudins and occludin were detected with specific Abs (Zymed).

Measurement of Paracellular Na and Cl Permeability. Cells were seeded into a Millicell-HA filter (12-mm diameter; Millipore). When the cells were confluent, expression of transgenes was induced for 4 days by the removal of doxycycline. Tracer-flux experiments were performed in a solution containing 150 mM NaCl, 5 mM KCl, 2 mM $CaCl_2$, 1.5 mM $MgCl_2$, and 10 mM

This paper was submitted directly (Track II) to the PNAS office.

Abbreviations: PHAII, pseudohypoaldosteronism type II; TSC, Na-dependent Cl cotransporter; MDCK II, Madin–Darby canine kidney II; HA, hemagglutinin.

*To whom correspondence should be addressed. E-mail: suchida.kid@tmd.ac.jp.

www.pnas.org/cgi/doi/10.1073/pnas.0306924101

Hepes·NaOH (pH 7.4). We added 1 μCi/ml (1 Ci = 37 GBq) ^{22}Na or 5 μCi/ml ^{36}Cl to the medium on one side of the membrane, and the appearance of radioactivity in the medium on the other side was measured at various times. The composition of medium on both sides of the membrane was identical. When ^{36}Cl was used, cold NaCl was added to the medium on the other side of the membrane because the concentration of NaCl in ^{36}Cl tracer was high (≈1.6 M). We measured ^{22}Na and ^{36}Cl activity with a gamma counter and a liquid scintillation counter, respectively. Permeabilities for ^{22}Na and ^{36}Cl were calculated by using the following equation: $J_{Cl} = C_{Cl} \times P_{Cl} \times A$, where J_{Cl} is transepithelial Cl flux (mol/s), C_{Cl} is concentration (mol/liter), A is surface area (cm^2), and P is permeability. Statistical comparison of multiple groups was assessed by ANOVA. Chloride permeabilities in the WNK4 expressing cells between uninduced and induced states were compared by using a paired t test. Error bars are represent mean ± SEM. Statistical significance was defined at $p < 0.05$.

Phosphorylation of Claudins. Mammalian expression vectors (3× Flag CMV14; Sigma) encoding Flag-tagged claudins and occludin were generated by RT-PCR. Both wild-type and mutant WNK4 expression vectors and claudin expression vectors were cotransfected into COS7 and MDCK II cells with Lipofectamine 2000 (Invitrogen). At 24 h after transfection, cells were incubated for 2 h in phosphate-free DMEM with 0.5% BSA and 10 mM Hepes (pH 7.4). The cells were incubated further for 2 h in the same medium containing [^{32}P]P_i (1 mCi/ml). After incubation, the cells were washed with phosphate-free DMEM, harvested, and lysed for 1 h on ice in 150 mM NaCl/15 mM Tris·HCl,/25 mM NaF/1 mM Na_3VO_4 (pH 8.0). Proteins were immunoprecipitated with anti-Flag M2 Ab. Western blot analyses of the immunoprecipitates were performed also by using an anti-Flag polyclonal Ab to confirm the expression of claudins. To detect the phosphorylation of endogenous claudins, immunoprecipitation of claudins in the WNK4-expressing MDCK II cells was performed by using anti-claudin 1 and 4 Abs (Zymed). Immunoprecipitated proteins were separated by SDS/PAGE, and phosphorylated proteins were visualized by autoradiography.

For *in vitro* kinase assays, a GST-fusion protein containing the kinase domain of WNK4 was generated by subcloning the *SalI–MstI* fragment of WNK4 into pGEX6P-1 (Amersham Biosciences). The cytoplasmic region of claudin 4 was also generated as a GST-fusion protein for uses as a substrate of WNK4. Protein kinase reactions were carried out at 30°C for 15 min in kinase buffer (10 mM Tris, pH 7.4/150 mM NaCl/10 mM $MgCl_2$/0.5 mM DTT). Reaction mixtures were resolved by SDS/PAGE, and phosphorylated proteins were visualized by autoradiography.

Coimmunoprecipitation of WNK4 and Claudins. HA-tagged WNK4 and Flag-tagged claudins expressed in COS7 and MDCK II cells were immunoprecipitated with anti-Flag M2 Ab, and coprecipitation was examined by Western blotting with an anti-HA Ab. The interaction of HA-WNK4 and endogenous tight-junction proteins in the WNK4-expressing MDCK II cells was examined by immunoprecipitation by using an anti-HA Ab, followed by Western blotting using Abs to tight-junction proteins (Zymed).

Results

WNK4 Increases Paracellular Cl Permeability in MDCK Cells. We generated stable MDCK II cell lines expressing the wild-type and one of the human disease-causing mutants (D564A) of WNK4 by using a tetracycline-inducible system. We measured the transepithelial paracellular ^{22}Na and ^{36}Cl permeability of these cells grown on a permeable support. Before measuring the Na and Cl permeability, expression of the wild-type and the mutant WNK4

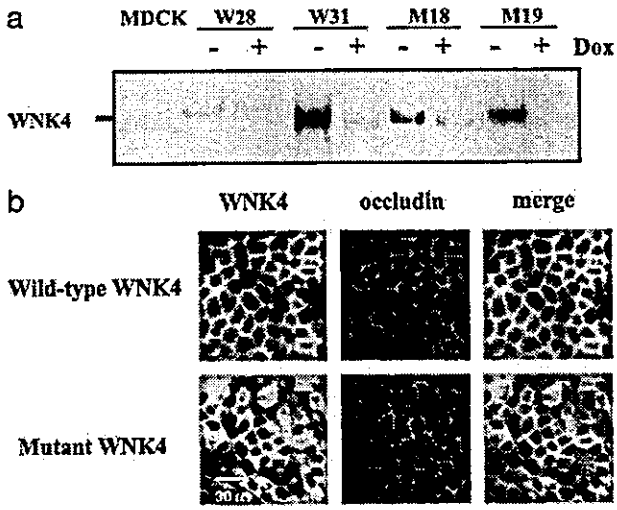

Fig. 1. Generation of wild-type and mutant WNK4-expressing MDCK II cell lines. (*a*) Expression of wild-type and mutant WNK4 in MDCK II cells. HA-tagged WNK4 proteins were detected by using an anti-HA (9Y10) Ab. Expression of WNK4 was induced by removal of doxycycline from the medium for 4 days. W28 and W31 are wild-type WNK4-expressing cell lines, and M18 and M19 are mutant WNK4-expressing cell lines. (*b*) Immunofluorescence of wild-type and mutant WNK4 expressed in isolated stable cell lines. Cells were grown on a permeable support, and the expression of WNK4 was induced for 4 days. WNK4 was detected by using an anti-HA Ab in conjunction with an Alexa 546-conjugated anti-rat IgG Ab. Cells were stained for occludin by using an anti-occludin Ab (Zymed) in conjunction with an Alexa 488-conjugated anti-rabbit IgG Ab.

were confirmed by Western blot analysis and immunofluorescence microscopy. As shown in Fig. 1*a*, stable cell lines expressing the wild-type and the mutant WNK4 were isolated. In all cell lines, some expression, even in the presence of doxycycline, was observed. Accordingly, we performed the initial experiments in induced cells (doxycycline-negative). Intracellular localization of the wild-type and the mutant WNK4 colocalized with the tight-junction protein occludin but did not appear to be different between the two cell lines (Fig. 1*b*). This localization of WNK4 in tight junctions is consistent with the reported (1) association of wild-type WNK4 with tight junctions *in vivo*. Flag-tagged WNK4 and HA-tagged WNK4 did not show the difference in terms of their cellular localization (data not shown).

We isolated several transformants after transfection with the empty vector, as well as the wild-type and mutant WNK4 cDNAs. We chose the four cell lines with the highest expression of the transgenes. Each cell line was cultured on a permeable support and was grown to confluence. Expression of WNK4 was induced for 4 days by removal of doxycycline from the medium. Transepithelial Na and Cl permeability were determined by assessing transepithelial ^{22}Na and ^{36}Cl flux across the epithelium. In these assays, the medium composition on both sides of the membrane was identical. Radioisotope was added to the basal side of the membrane, and the appearance of radioisotope in the apical medium was measured over time. Our preliminary experiments revealed that Na and Cl flux was linear for 45 min. Therefore, we adopted 30 min as an incubation time for subsequent experiments. The calculated basal to apical permeability was identical to the apical to basal permeability. Addition of 1 mM ouabain/0.1 mM bumetanide/0.1 mM amiloride/0.1 mM hydrochlorothiazide/1 mM 4,4′-diisothiocyanatostilbene-2,2′-disulfonic acid/1 mM 4-acetamido-4′-isothiocyanatostilbene-2,2′-disulfonic acid had no effect on Na or Cl flux. In addition, Na and Cl fluxes measured in this assay appeared not to saturate

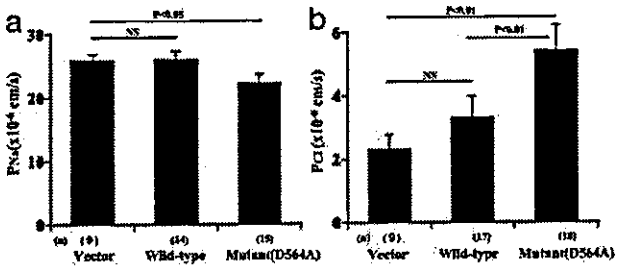

Fig. 2. Transepithelial ^{22}Na (*a*) and ^{36}Cl (*b*) permeability in MDCKII cells expressing wild-type and mutant WNK4. Each bar represents experiments using at least three cell lines. The numbers of assays are given in parentheses. At least three assays were performed with each cell line.

as a function of NaCl concentration up to 200 mM. These results (see Figs. 6 and 7, which are published as supporting information on the PNAS web site) suggest that our measurements represent paracellular Na and Cl permeability of the epithelium. Our permeability calculations [P (Na) = 25.8 ± 0.9 cm/s (mean ± SEM, n = 7), P (Cl) = 2.0 ± 0.3 cm/s (mean ± SEM, n = 11) in the host cells] also agreed with calculations made previously by using other methods (10). These calculated permeabilities suggest that our simplified assay is valid for measuring transepithelial Na and Cl permeability.

As shown in Fig. 2*a*, Na permeability was not changed by the expression of the wild-type WNK4 compared with the vector transfection. However, the mutant WNK4 causes a statistically significant decrease in Na permeability ($p < 0.05$). The Cl permeability in the wild-type WNK4-expressing cell lines tended to be increased over the control (empty-vector transfectants), but the difference was not statistically significant. In the two wild-type WNK4-transfected cell lines that showed the least leaky WNK4 expression in the presence of doxycycline, chloride permeabilities under induced and noninduced conditions were not statistically different. On the other hand, the mutant WNK4 caused an apparent increase in Cl permeability ($p < 0.01$) over the control and also over the wild type ($p < 0.01$). This increase of chloride permeability was not due to a general increase of permeability of the epithelia because Na permeability was reduced. To further confirm that the increase in chloride permeability in the mutant WNK4-expressing cells correlated with the expression of the mutant WNK4, we chose the two mutant WNK4-transfected cell lines that showed the least leaky WNK4 expression. In those cells, chloride permeability under the induced and noninduced conditions was 5.8 ± 0.4 and 2.8 ± 0.2 ($\times 10^{-6}$ cm/s), respectively, which were statistically significant (mean ± SEM, n = 6, $p < 0.01$).

Effect of WNK4 Expression on Cellular Localization of Tight-Junction Proteins. We suspected that WNK4 expression enhanced Cl permeability by modifying proteins in the tight junction. We first performed immunofluoresence and Western blot analyses of tight-junction proteins to determine whether there was any difference in expression or localization. Fig. 3*a* shows the immunofluorescence staining for several claudins and occludin. The localization of these proteins in the tight junctions did not appear to be affected by wild-type or mutant WNK4 expression. Because the recruitment of some proteins to the tight junctions, including occludin, claudins, and ZO-1, are regulated by various signals (11), we examined their distribution in the Triton X-100-soluble (cytosol) and -insoluble (cytoskeleton and tight junctions) cellular fractions by Western blotting. As shown in Fig. 3*b*, the distribution of the claudins into Triton X-100-insoluble fraction was not significantly altered by the expression of wild-type or mutant WNK4, although two of four wild-type WNK4–

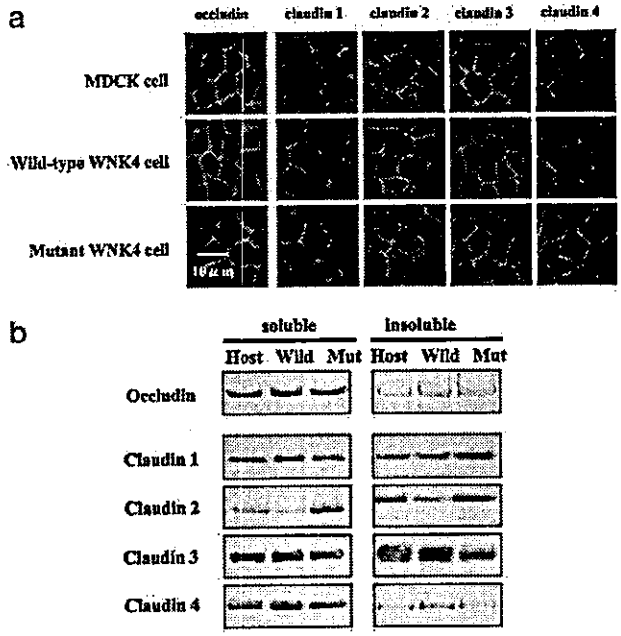

Fig. 3. Tight-junction proteins in WNK4-expressing cells. (*a*) Immunofluorescence of tight-junction proteins in the WNK4-expresing cells. Stable WNK4-expressing cell lines were grown on a permeable support. Cells were immunostained with anti-claudin 1–4 Abs or with an anti-occludin Ab. (*b*) Expression of claudins and occludin in Triton X-100-soluble and -insoluble fractions in WNK4-expressing cells. WNK4 expression was induced for 4 days, and cells were harvested in a buffer containing 1% Triton X-100. The Triton X-100-soluble and -insoluble fractions were resolved by SDS/PAGE, and the expression of claudins and occludin were determined by Western blot analysis.

expressing cell lines displayed decreased claudin 2 expression. A similar reduction in claudin 2 expression was reported (12) in cells overexpressing claudin 8, although that was thought to be an artifact of overexpression. We, therefore, concluded that the increased Cl permeability in WNK4-expressing cells was not caused by changes in the recruitment of tight-junction proteins.

Increased Phosphorylation of Claudins Induced by WNK4 Overexpression. We next investigated whether the change in Cl permeability was associated with modification of the tight-junction proteins (i.e., phosphorylation). Because commercially available Abs for claudins are not always effective for immunoprecipitation, we initially examined the phosphorylation of Flag-tagged claudins. We first used COS7 cells to obtain consistent expression of exogenous claudins. Fig. 4*a* shows that all claudins tested (claudin 1–4) were phosphorylated in cells expressing WNK4. Cells expressing mutant WNK4 contained a higher level of phosphorylated claudin than cells expressing wild-type WNK4. Occludin, an endogenously phosphorylated tight-junction protein, was not phosphorylated further in cells expressing either the wild-type or the mutant WNK4. Less phosphorylation of claudins by the wild-type WNK4 than the mutant, and the lack of further phosphorylation of occludin by WNK4 suggested that the phosphorylation of claudins by the mutant WNK4 was not due to an artifact of overexpression. The same results were obtained in MDCK II cells (Fig. 4*b*). To further confirm these results, we also checked the phosphorylation of endogenous claudins in the WNK4-expressing MDCK cells. As shown in Fig. 4*c*, endogenous claudin 1 and claudin 4 were apparently phosphorylated in the mutant-expressing MDCK II cells, identifying a putative molecular target for this protein kinase. We also examined the level of WNK4 phosphorylation because WNK1 is known to autophos-

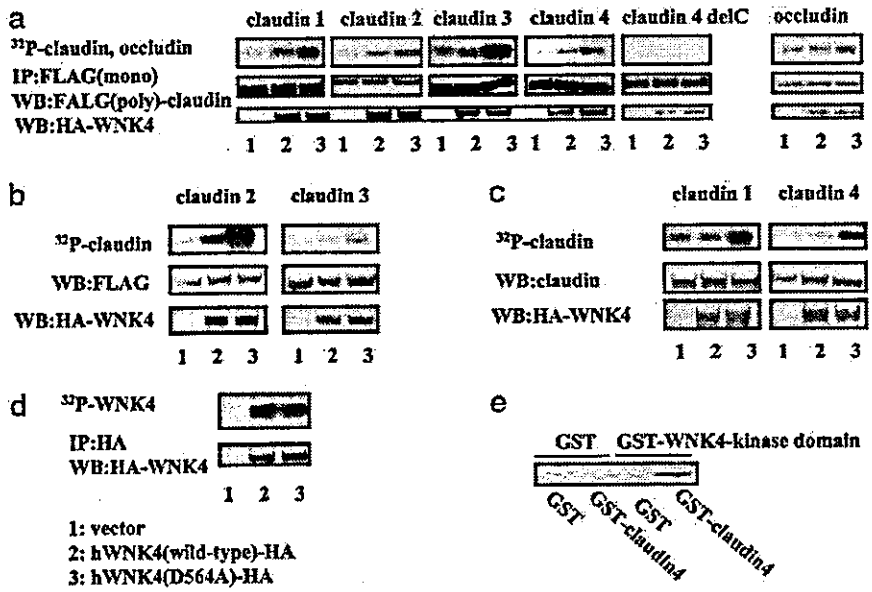

Fig. 4. Phosphorylation of claudins by WNK4. (*a*) Phosphorylation of Flag-tagged claudins by WNK4 in COS7 cells. COS7 cells were transfected with HA-tagged WNK4 and Flag-tagged claudins or occuludin. Claudin 4 delC lacks the entire C-terminal cytosolic region of claudin4. Cells were labeled with [^{32}P]P_i (1 mCi/ml), and proteins were immunoprecipitated with an anti-Flag Ab (M2). The immunoprecipitated Flag-claudins were separated by SDS/PAGE, electrophoretically transferred to nitrocellulose, and analyzed by Western blotting with an anti-Flag polyclonal Ab. After detecting the immunoprecipitated claudins, claudin phosphorylation was detected by autoradiography of the nitrocellulose membrane. (*b*) Phosphorylation of Flag-tagged claudins in the WNK4-expressing MDCK II cells. MDCK II cells stably expressing HA-tagged WNK4 were transfected with Flag-tagged claudin 2 and 3. Phosphorylated claudin 2 and 3 were detected, as described in a. (*c*) Phosphorylation of endogenous claudins in the mutant WNK4-expressing MDCK II cells. The WNK4-expressing cells were labeled with [^{32}P]P_i, and the endogenous claudins were immunoprecipitated by using anti-claudin 1 and 4 Abs (Zymed). Phosphorylation of claudins was visualized by autoradiography. (*d*) Phosphorylation of wild-type and mutant WNK4. MDCK II cells were transfected with HA-tagged wild-type and mutant WNK4. Cells were labeled with [^{32}P]P_i, and WNK4 proteins were immunoprecipitated with an anti-HA Ab. Immunoprecipitated proteins were resolved on SDS/PAGE, electrophoretically transferred to nitrocellulose, and analyzed by Western blotting with an anti-HA Ab. WNK4 phosphorylation was detected by autoradiography. (*e*) *In vitro* kinase assay with GST-WNK4. GST-WNK4 (kinase domain) and GST–claudin 4 (C-terminal cytoplasmic domain) were incubated at 37°C for 15 min in kinase buffer, and the phosphorylation of GST–claudin 4 was visualized by SDS/PAGE, followed by autoradiography.

phorylate (13, 14). As shown in Fig. 4*d*, there was an equal level of phosphorylation on wild-type and mutant WNK4. Finally, to verify that claudins were direct substrates for WNK4, we performed an *in vitro* kinase assay by using recombinant GST-fusion proteins of the kinase domain of WNK4 and the cytoplasmic domain of claudin 4. As shown in Fig. 4*e*, WNK4 directly phosphorylated the cytoplasmic domain of claudin 4.

Protein–Protein Interaction of WNK4 and Claudins. Our results clearly show that WNK4, especially the mutant WNK4, can phosphorylate claudins. Moreover, it appears that the mutant WNK4 has an enhanced ability to phosphorylate these proteins. To investigate this possibility further, we first examined whether WNK4 associates with the claudins. As expected from the phosphorylation study, claudins and WNK4 coimmunoprecipitated (Fig. 5*a*). The mutant WNK4 showed a much higher association with claudins than the wild-type WNK4. Because our analyses of WNK4 phosphorylation suggested that the wild-type and mutant proteins possess the same level of autophosphorylation (Fig. 4*d*) and, therefore, the same kinase activities, it appears that the enhanced phosphorylation of claudins by mutant WNK4 is due to the increased claudin–WNK4 association. Interaction of the mutant WNK4 with the endogenous claudin 1 and 4 but not with ZO-1 and occludin was confirmed in the mutant-expressing MDCK II cells (Fig. 5*b*).

In our phosphorylation studies (Fig. 4*a*), we found that deletion of the entire cytoplasmic C terminus of claudin 4 eliminated its phosphorylation, suggesting that the C terminus is the site of phosphorylation and/or binding by WNK4. Fig. 5*c* confirms that this C-terminal deletion mutant lost its ability to bind to the mutant WNK4, but that the addition of the C-terminal YV, a sequence highly conserved in all claudins (a binding site to PDZ domains of ZO-1, 2, and 3) (15), restored binding to the mutant WNK4. This finding indicates that the YV sequence is necessary for claudin binding and explains the fact that the mutant WNK4 binds all of the claudins tested. Phosphorylation of this mutant was not restored by the addition of YV motif (data not shown), suggesting that phosphorylation sites were present within the cytosolic C terminus.

Discussion

Two findings are presented in this article. First, we identified claudins as molecular targets of the protein kinase WNK4, especially the disease-causing mutant WNK4. Second, we show that paracellular ion permeability is regulated by the mutant WNK4. This study characterizes WNK4 expressed in polarized epithelial cells, and both data are quite consistent with the *in vivo* localization of WNK4 and the chloride shunt hypothesis in PHAII.

A growing body of evidence, including genetic (16) and cell biological (10, 12, 17–20) data, has suggested that paracellular transepithelial transport is important in vectorial ion and solute transport across the epithelia. Thus, it appears that, like channels, paracellular transport possesses selectivity for ions and solutes. Although several lines of evidence have suggested that claudins are the major determinants of paracellular ion selectivity (10, 12, 17–20), their phosphorylation has not, to our knowledge, been demonstrated. Our data showed a good correlation between increased chloride permeability and claudin phosphorylation induced by the mutant WNK4, suggesting that

PHYSIOLOGY

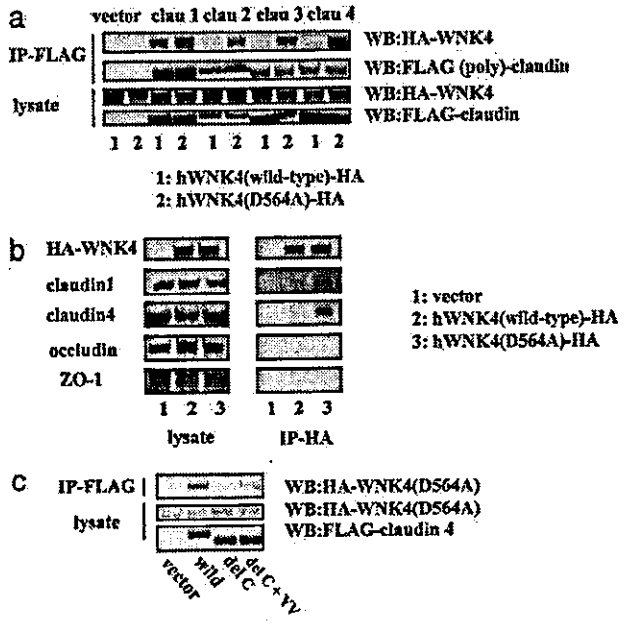

Fig. 5. Analysis of WNK4–claudin interaction. (*a*) Coimmunoprecipitation of WNK4 and claudins. COS7 cells were transfected with HA-tagged WNK4 and Flag-tagged claudins. Proteins were immunoprecipitated with an anti-Flag M2 Ab, and the immunoprecipitates were analyzed by Western blot analysis by using anti-HA Ab. (*b*) Coimmunoprecipitation of WNK4 and endogenous tight-junction proteins. Proteins from MDCK II cells stably expressing the wild-type and mutant HA-WNK4 were immunoprecipitated with anti-HA Ab, and the immunoprecipitates were analyzed by Western blot analysis by using Abs to claudin 1, claudin 4, ZO-1, and occludin. (*c*) Binding of claudin 4 and its mutants by mutant WNK4. Claudin 4 binding was assessed by coimmunoprecipitation in lysates from MDCK II cells as described in *a*. Mutants examined include delC (the claudin 4 mutant lacking the entire C terminal cytoplasmic region) and del C plus YV (the del C mutant with Y and V added to the C terminus). Addition of YV residues restored the binding to WNK4.

the two phenomena are related causally. However, whether the phosphorylation of claudins causes an increase in the chloride permeability directly remains to be determined. A mutagenesis study showed that the extracellular domain of claudin controls paracellular charge selectivity and resistance (10). However, it is not clear now whether the phosphorylation of the cytoplasmic domain affects chloride permeability. Currently, there is no good system, to our knowledge, for assaying the function of exogenously expressed claudins in mammalian cells because of the presence of numerous endogenous claudins. We can only speculate that the phosphorylation by WNK4 affects the conformation of claudins, increasing Cl ion pore permeability or affecting their interaction with intracellular regulators, such as cytoskeletal proteins.

We found in this study that the disease-causing mutation in WNK4 has a gain-of-function effect, causing increased chloride permeability and hyperphosphorylation of claudins. This finding provides a good explanation for the autosomal-dominant nature of inheritance in PHAII. Very recently, Kahle *et al.* (6) reported the inhibition of surface expression of the renal K^+ channel ROMK by coexpression of wild-type WNK4 in *Xenopus* oocytes. Interestingly, a disease-causing mutation in WNK4 that relieves TSC inhibition (4, 5) markedly increases inhibition of ROMK. This difference in the action of the mutant WNK4 on TSC and ROMK indicates that WNK4 functions as a multifunctional regulator of diverse ion transporters. Identification of functions of WNK4 in this study further supports this notion. However, how this mutation increases WNK4 activity is not clear, as in the case of ROMK inhibition. In terms of claudin phosphorylation, one possible explanation for the enhanced effect of the mutant is change in the binding to claudins. In fact, Xu *et al.* (14) recently reported the presence of an autoinhibitory domain in WNK1 that resides near the coil domain. Interestingly, PHAII-causing mutations are concentrated near the putative autoinhibitory domain of WNK4. Therefore, it is possible that the disease-causing mutations in WNK4 somehow affect its interaction with its negative regulators including its own domains, releasing the active site, and allowing enhanced binding to claudins. Although we show that YV motif of claudins is important for the interaction with WNK4, further work will be required to define the whole mechanisms of their interaction.

In this article, we identified the claudins as targets of WNK4 kinase and showed that the disease-causing mutant WNK4 expression increases paracellular chloride permeability without increasing sodium permeability. A similar phenomenon may occur in the collecting ducts of PHAII patients. Therefore, increased chloride shunt caused by a gain-of-function activity of mutant WNK4 may underlie or contribute to the pathogenesis of PAHII.

We thank H. Ichijo (Tokyo University) for his excellent advice. This study was supported in part by grants-in-aid from the Ministry of Education, Culture, Sports, Science, and Technology of Japan and the Salt Science Research Foundation.

1. Wilson, F. H., Disse-Nicodeme, S., Choate, K. A., Ishikawa, K., Nelson-Williams, C., Desitter, I., Gunel, M., Milford, D. V., Lipkin, G. W., Achard, J. M., *et al.* (2001) *Science* **293**, 1107–1112.
2. Schambelan, M., Sebastian, A. & Rector, F. C., Jr. (1981) *Kidney Int.* **19**, 716–727.
3. Farfel, Z., Iaina, A., Rosenthal, T., Waks, U., Shibolet, S. & Gafni, J. (1978) *Arch. Intern. Med. (Moscow)* **138**, 1828–1832.
4. Wilson, F. H., Kahle, K. T., Sabath, E., Lalioti, M. D., Rapson, A. K., Hoover, R. S., Hebert, S. C., Gamba, G. & Lifton, R. P. (2003) *Proc. Natl. Acad. Sci. USA* **100**, 680–684.
5. Yang, C. L., Angell, J., Mitchell, R. & Ellison, D. H. (2003) *J. Clin. Invest.* **111**, 1039–1045.
6. Kahle, K. T., Wilson, F. H., Leng, Q., Lalioti, M. D., O'Connell, A. D., Dong, K., Rapson, A. K., MacGregor, G. G., Giebisch, G., Hebert, S. C. & Lifton R. P. (2003) *Nat. Genet.* **35**, 372–376.
7. Schuster, V. L. & Stokes, J. B. (1987) *Am. J. Physiol.* **253**, F203–F212.
8. Plotkin, M. D., Kaplan, M. R., Verlander, J. W., Lee, W. S., Brown, D., Poch, E., Gullans, S. R. & Hebert, S. C. (1996) *Kidney Int.* **50**, 174–183.
9. Xu, J. Z., Hall, A. E., Peterson, L. N., Bienkowski, M. J., Eessalu, T. E. & Hebert, S. C. (1997) *Am. J. Physiol.* **273**, F739–F748.
10. Colegio, O. R., Itallie, C. V., Rahner, C. & Anderson, J. M. (2003) *Am. J. Physiol.* **284**, C1346–C1354.
11. Nishiyama, R., Sakaguchi, T., Kinugasa, T., Gu, X., MacDermott, R. P., Podolsky, D. K. & Reinecker, H. C. (2001) *J. Biol. Chem.* **276**, 35571–35580.
12. Yu, A. S., Enck, A. H., Lencer, W. I. & Schneeberger, E. E. (2003) *J. Biol. Chem.* **278**, 17350–17359.
13. Xu, B., English, J. M., Wilsbacher, J. L., Stippec, S., Goldsmith, E. J. & Cobb, M. H. (2000) *J. Biol. Chem.* **275**, 16795–16801.
14. Xu, B. E., Min, X., Stippec, S., Lee, B. H., Goldsmith, E. J. & Cobb, M. H. (2002) *J. Biol. Chem.* **277**, 48456–48462.
15. Itoh, M., Furuse, M., Morita, K., Kubota, K., Saitou, M. & Tsukita, S. (1999) *J. Cell Biol.* **147**, 1351–1363.
16. Simon, D. B., Lu, Y., Choate, K. A., Velazquez, H., Al-Sabban, E., Praga, M., Casari, G., Bettinelli, A., Colussi, G., Rodriguez-Soriano, J., *et al.* (1999) *Science* **285**, 103–106.
17. Amasheh, S., Meiri, N., Gitter, A. H., Schoneberg, T., Mankertz, J., Schulzke, J. D. & Fromm, M. (2002) *J. Cell Sci.* **115**, 4969–4976.
18. Colegio, O. R., Van Itallie, C. M., McCrea, H. J., Rahner, C. & Anderson, J. M. (2002) *Am. J. Physiol.* **283**, C142–C147.
19. Furuse, M., Furuse, K., Sasaki, H. & Tsukita, S. (2001) *J. Cell Biol.* **153**, 263–272.
20. Van Itallie, C., Rahner, C. & Anderson, J. M. (2001) *J. Clin. Invest.* **107**, 1319–1327.

Research article

Inhibition of diabetic nephropathy by a decoy peptide corresponding to the "handle" region for nonproteolytic activation of prorenin

Atsuhiro Ichihara,[1] Matsuhiko Hayashi,[1] Yuki Kaneshiro,[1] Fumiaki Suzuki,[2,3] Tsutomu Nakagawa,[2] Yuko Tada,[1] Yukako Koura,[1] Akira Nishiyama,[4] Hirokazu Okada,[5] M. Nasir Uddin,[2] A.H.M. Nurun Nabi,[3] Yuichi Ishida,[6] Tadashi Inagami,[7] and Takao Saruta[1]

[1]Department of Internal Medicine, Keio University School of Medicine, Tokyo, Japan. [2]Faculty of Applied Biological Sciences, [3]United Graduate School of Agricultural Science, Gifu University, Gifu, Japan. [4]Department of Pharmacology, Kagawa Medical School, Kagawa, Japan. [5]Nephrology, Saitama Medical College, Saitama, Japan. [6]Prevaqol Co., Tokyo, Japan. [7]Department of Biochemistry, Vanderbilt University School of Medicine, Nashville, Tennessee, USA.

We found that when a site-specific binding protein interacts with the "handle" region of the prorenin prosegment, the prorenin molecule undergoes a conformational change to its enzymatically active state. This nonproteolytic activation is completely blocked by a decoy peptide with the handle region structure, which competitively binds to such a binding protein. Given increased plasma prorenin in diabetes, we examined the hypothesis that the nonproteolytic activation of prorenin plays a significant role in diabetic organ damage. Streptozotocin-induced diabetic rats were treated with subcutaneous administration of handle region peptide. Metabolic and renal histological changes and the renin-Ang system components in the plasma and kidneys were determined at 8, 16, and 24 weeks following streptozotocin treatment. Kidneys of diabetic rats contained increased Ang I and II without any changes in renin, Ang-converting enzyme, or angiotensinogen synthesis. Treatment with the handle region peptide decreased the renal content of Ang I and II, however, and completely inhibited the development of diabetic nephropathy without affecting hyperglycemia. We propose that the nonproteolytic activation of prorenin may be a significant mechanism of diabetic nephropathy. The mechanism and substances causing nonproteolytic activation of prorenin may serve as important therapeutic targets for the prevention of diabetic organ damage.

Introduction

The most striking abnormalities of the renin-Ang system (RAS) in the blood of diabetic animals are the decreased renin level and the increased prorenin level (1). Indeed, increased blood prorenin levels in human diabetics have been reported to predict microvascular complications (2). Recent studies have demonstrated that transgenic rats expressing prorenin have severe renal histopathology mimicking diabetic nephrosclerosis without hypertension (3) and show evidence that circulating prorenin may enter organs (4). The mechanism whereby intracellular prorenin causes organ damage remained unclear, however.

Prorenin has a prosegment of 43 amino acid residues attached to the N terminus of mature (active) renin, and the prosegment folds into an active site cleft of mature renin to prevent catalytically productive interaction with angiotensinogen. When a prorenin-binding protein interacts with the "handle" region of the prorenin prosegment, the prorenin molecule undergoes a conformational change to an enzymatically active state (5). This phenomenon is called nonproteolytic activation, and such binding proteins include a specific Ab to the prosegment (5), the *N*-acyl-D-glucosamine 2-epimerase (6), the mannose-6-phosphate receptor (7, 8), or the prorenin/renin receptor (9). These findings indicate the strong possibility that a peptide with the structure of this handle region (handle region peptide, or HRP; see Figure 1) must competitively bind to such a binding protein as a decoy peptide and inhibit the nonproteolytic activation of prorenin.

In the present study, we used such a decoy peptide to demonstrate a novel mechanism whereby prorenin as such, without proteolytic activation, causes organ damage by comparing levels of the RAS components in the kidney and plasma during the development of diabetic nephropathy. HRP clearly prevented development of diabetic nephropathy and suppressed an increase of renal Angs while the total renal renin plus prorenin remained unaltered. To clarify the mechanism whereby prorenin causes organ damage, we investigated the alteration of the RAS component levels in the plasma and kidneys during the development of diabetic nephropathy and the in vitro and in vivo effects of HRP on their alteration levels.

Results

In vitro effects of HRP on binding of prorenin to prorenin Abs. To examine the affinity, specificity, and dose of HRP in the inhibitory effects on the binding of rat prorenin to its Abs, immunoblot analysis of recombinant prorenin to the Ab for the anti-handle region was performed. The binding of recombinant prorenin to the Ab for the anti-handle region was completely inhibited by 1 μM HRP (RILLKKMPSV) but was not influenced by the peptides representing other regions of the prorenin prosegment (SFGR or MTRISAE) (Figure 2A). Similar results were also obtained at 10 and 100 nM HRP. In

Nonstandard abbreviations used: ACE, Ang-converting enzyme; C rat, nondiabetic control rat with saline minipump; C + HRP rat, nondiabetic control rat with HRP-containing minipump; DM + HRP rat, diabetic rat with HRP minipump; DM rat, diabetic rat with saline-containing minipump; HRP, handle region peptide; RAS, renin-Ang system.

Conflict of interest: The authors have declared that no conflict of interest exists.

Citation for this article: *J. Clin. Invest.* 114:1128–1135 (2004). doi:10.1172/JCI200421398.

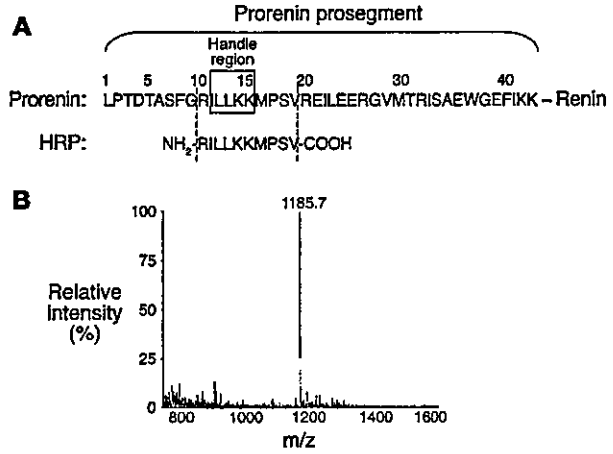

Figure 1
Preparation of the decoy peptide corresponding to the HRP. (**A**) Amino acid sequences of the rat prorenin prosegment and HRP. (**B**) Mass of the HRP prepared.

addition, HRP did not affect the binding of prorenin to Ab against proteolytically activated renin (Figure 2B). These results suggest that HRP can specifically bind to the anti-HRP Ab with a high affinity and inhibit the binding of prorenin to anti-HRP Ab in vitro.

During in vitro preliminary experiments, we had expressed rat prorenin/renin receptor protein (accession number AB188298 in the DNA Databank of Japan) in COS-7 cells and showed binding and activation of recombinant rat prorenin by 20% ± 2.5% of the trypsin-activatable level (350 ng Ang I/ml/hr). This activation was practically abolished by rat HRP (10P–19P) used as a decoy at 1 μM, but not by another prosegment heptapeptide (30P–36P) outside the handle region, indicating specific inhibitory action of HRP against prorenin activation. We also found that prorenin activated by rat prorenin/renin receptor expressed on COS-7 cells could be bound to anti-rat HRP Abs on the cells, visualized by using intensifying second Ab conjugated with peroxidase. This result indicated that prorenin activated by the receptor protein still had a prosegment including the handle region and that activation of prorenin by the receptor protein was presumably not due to a proteolytic mechanism but was due to a conformational change. Analogous to the prorenin/renin-binding protein, polyclonal Abs to the rat HRP also activated rat prorenin by 20% ± 1.0% of the maximum activation attainable by trypsin, and the activation was practically abolished by 1 μM HRP used as a decoy. These results indicate that specific binding of prorenin either to the receptor protein or Ab to HRP results in a significant activation of prorenin. These observations provide in vitro evidence that HRP inhibits the activation by competing out the binding of the prorenin receptor or HRP Abs to prorenin.

Metabolic changes and urinary protein excretion. We determined metabolic changes and urinary protein excretion in nondiabetic control rats with saline minipumps (C rats), nondiabetic control rats with HRP-containing minipumps (C + HRP rats), diabetic rats with saline-containing minipumps (DM rats), and diabetic rats with HRP minipumps (DM + HRP rats) during the 24-week treatment period (Figure 3). The body weight of the DM rats averaged 231 ± 15 g at 28 weeks of age and was significantly smaller than that of the C rats (590 ± 10 g). The basal BP of the C and DM rats averaged 123 ± 2 and 122 ± 2 mmHg, respectively, and the BP had been similar in the C and DM rats during the 24-week treatment period. The blood glucose levels of the DM rats averaged 509 ± 34 mg/dl at 8 weeks of age (4 weeks of diabetes) and was significantly higher than those of the C rats (132 ± 14 mg/dl). Higher blood glucose levels of the DM rats versus the C rats were maintained during the 24-week treatment period. Continuous infusion of HRP by subcutaneous minipumps did not affect the body weight, BP, or blood glucose levels of either control or diabetic rats during the 24-week treatment period, although the body weight of diabetic rats increased at 24 and 28 weeks of age. In the DM rats, urinary protein excretion significantly increased from 20.0 ± 3.1 at 4 weeks of age (0 weeks of diabetes) to 118.8 ± 11.9 mg/day at 28 weeks of age (24 weeks of diabetes), and HRP practically normalized the increased urinary protein excretion in diabetic rats to levels similar to those of the control rats. The urinary protein excretion at 28 weeks of age (24 weeks of diabetes) in the DM + HRP rats averaged 33.0 ± 4.1 mg/day and was similar to that in the C and C + HRP rats.

Morphology and immunohistochemistry. Figure 4A shows changes in renal morphology in the C, C + HRP, DM, and DM + HRP rats during the 24-week treatment period. We did not observe any histological changes in the kidney of the DM rats up to 12 weeks of age (8 weeks of diabetes), but glomerulosclerosis began to develop at 20 weeks of age (16 weeks of diabetes) and was exacerbated at 28 weeks of age (24 weeks of diabetes). As shown in Figure 4B, the glomerulosclerosis index of 20- and 28-week-old DM rats averaged 1.25 ± 0.16 and 1.96 ± 0.14, respectively, and was significantly greater than that of the C, C + HRP, or DM + HRP rats. In the 28-week-old DM rats, the glomerulosclerosis index was significantly greater than that at 20 weeks of age. Long-term administration of HRP completely inhibited the development of glomerulosclerosis in the diabetic rats, and we did not observe any histological changes during the 24-week treatment period in the DM + HRP rats.

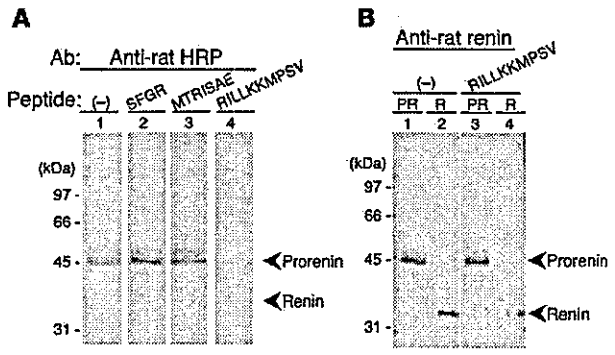

Figure 2
Interference of the prorenin binding to its Abs by the HRP. (**A**) Recombinant rat prorenin was analyzed by immunoblotting using 3 nM purified Ab to HRP in the absence (–; lane 1) or presence of 1 μM regional peptides of prorenin prosegment, SFGR (lane 2), MTRISAE (lane 3), or RILLKKMPSV (lane 4). The image shows that HRP binds to the anti–HRP Ab with a high affinity and inhibits the binding of recombinant prorenin to anti–HRP Ab. Similar results were also obtained at 10 and 100 nM RILLKKMPSV. (**B**) Recombinant rat prorenin (PR) (lanes 1 and 3) and renin (R) (lanes 2 and 4) were analyzed by immunoblotting using anti–rat renin Ab in the absence (lanes 1 and 2) or presence of 1 μM HRP, RILLKKMPSV (lanes 3 and 4). The image shows that HRP specifically binds to the anti–HRP Ab but not to the anti–renin Ab and does not inhibit the binding of prorenin to anti–renin Ab.

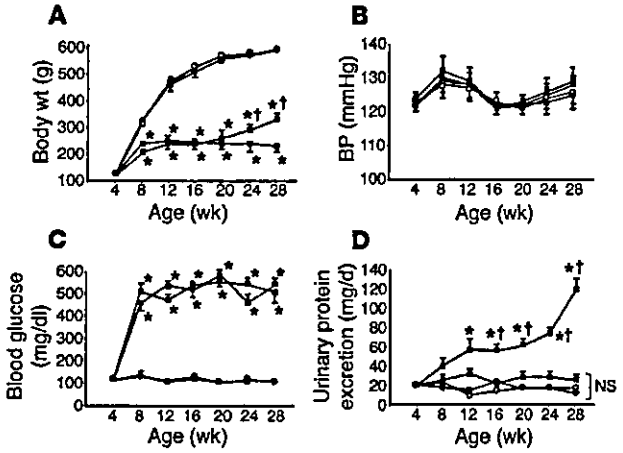

Figure 3

Metabolic changes and urinary protein excretion in C rats (open circles, $n = 18$), C + HRP rats (closed circles, $n = 18$), DM rats (open squares, $n = 18$), and DM + HRP rats (closed squares, $n = 18$). (**A**) Body weight. Graph shows attenuation of body weight gain in diabetic rats. Except for the increases at 24 and 28 weeks of age in diabetic rats, HRP did not affect body weight during the 24-week treatment period. *$P < 0.05$ versus C or C + HRP rats; †$P < 0.05$ for DM + HRP versus DM rats. (**B**) Systolic BP. The graph shows similar systolic BP in all 4 groups of rats. (**C**) Blood glucose concentration. The graph shows increased blood glucose levels in the diabetic rats. HRP had no effect on blood glucose levels. *$P < 0.05$ versus C or C + HRP rats. (**D**) Urinary protein excretion. The graph shows a progressive increase in urinary protein excretion in DM rats. HRP treatment inhibited the development and progression of proteinuria in diabetic rats. *$P < 0.05$ versus 4 weeks of age; †$P < 0.05$ for DM rats versus the other 3 groups. NS, no significant difference among the C, C + HRP, and DM + HRP rats.

The glomerulosclerosis index was similar among the C, C + HRP, and DM + HRP rats during the 24-week treatment period. We also investigated ECM accumulation in the kidney of diabetic rats by type IV collagen immunostaining, as shown in Figure 4C. Kidneys of all groups of rats were negative for expression of type IV collagen in the glomerulus up to 12 weeks of age, but at 20 weeks of age type IV collagen was expressed in the glomerulosclerotic lesions of the kidneys of the DM rats. At 28 weeks of age, expression of type IV collagen increased in the DM rats, but it was markedly suppressed to a level slightly higher than the control level in the DM + HRP rats ($n = 6$), though the difference between C rats and DM + HRP rats was statistically insignificant (Figure 4D). Expression of type IV collagen during the 24-week treatment period was not observed in either the C or C + HRP rats.

Components of the circulating and kidney RAS. As shown in Figure 5, plasma renin activity was significantly lower in the DM rats than in the C rats during the 24-week treatment period, and administration of HRP did not affect plasma renin activity in either control or diabetic rats (Figure 5A). Plasma prorenin level was significantly higher in the DM rats than in the C rats up to 20 week of age (16 weeks of diabetes), and administration of HRP did not affect plasma prorenin level in either control or diabetic rats (Figure 5B). The plasma levels of Ang I and II were also lower in the DM rats than in the C rats during the 24-week treatment period, and HRP did not influence plasma Ang I or II levels of either control or diabetic rats (Figure 5, C and D).

At 8 weeks of age (4 weeks of diabetes) when the diabetic nephropathy had not yet developed, the DM rats had a small but significant increase in the kidney Ang I and II content (109 ± 16 and 147 ± 12 fmol/g, respectively) compared with the C rats (58 ± 11 and 77 ± 8 fmol/g, respectively). At 12, 20, and 28 weeks of age, the kidney Ang I and II content was significantly higher in the DM rats than the similarly low levels in the C, C + HRP, and DM + HRP rats (Figure 6, A and B). The kidney Ang I content of the DM, DM + HRP, C, and C + HRP rats averaged 268 ± 51, 70 ± 8, 88 ± 14, and 71 ± 13 fmol/g, respectively, and the kidney Ang II content of the DM, DM + HRP, C, and C + HRP rats averaged 220 ± 21, 126 ± 15, 148 ± 14, and 124 ± 12 fmol/g, respectively, at 20 weeks of age (16 weeks of diabetes) when renal histological changes have developed. Thus, HRP administration completely inhibited the increased kidney Ang I and II content in the diabetic rats. The kidney total renin content and the kidney renin mRNA level were lower in the DM rats than in the C rats at 12 and 20 weeks of age, and they were similar at 28 weeks of age. HRP administration did not alter kidney total renin content or kidney renin mRNA levels in either control or diabetic rats at any week of age (Figures 6C and 7A). The kidney Ang-converting enzyme (ACE) and angiotensinogen mRNA levels were similar in the C, C + HRP, DM, and DM + HRP rats during the 24-week treatment period (Figure 7, B and C) but tended to decrease with age. The kidney cathepsin B mRNA level was significantly lower in the DM rats than in the C rats during the 24-week treatment period. HRP administration did not alter kidney cathepsin B mRNA level in either control or diabetic rats at any week of age (Figure 7D).

To estimate the kidney levels of prorenin and renin, we performed immunohistochemical analysis of the kidneys collected from rats diabetic for 24 weeks. The anti-rat HRP Ab and anti-rat renin Ab used in the present study bind to total prorenin and activated prorenin, respectively. Because the activated prorenin represents both proteolytically activated prorenin (i.e., renin) and nonproteolytically activated prorenin, the results of immunostaining can provide a hint regarding an activation of prorenin. The prorenin-positive cells were significantly greater in number in the juxtaglomerular area of DM rats compared with C rats. The increased prorenin immunoreactivity was not affected by the HRP treatment (Figure 8, A and B). The immunoreactivity of activated prorenin was also increased in the juxtaglomerular area of DM rats, but it was significantly decreased by the HRP treatment. The level of activated prorenin in the kidneys of DM + HRP rats was similar to that in the kidneys of C and C + HRP rats (Figure 8, A and C). Because HRP inhibited a nonproteolytic activation of prorenin but did not affect a renin that is proteolytically activated prorenin (Figure 2B), these results suggested that the kidneys of DM rats may have an increased level of nonproteolytically activated prorenin. Although localization of renin in the distal nephron has been reported, we were not able to detect a significant staining by anti-HRP or anti-renin in the tubulointerstitial area in the present study, presumably due to very low level of these nephron segments compared with the juxtaglomerular area that can be seen in the sections.

Discussion

We found that the rat HRP binds to the Abs to the handle region of the prorenin prosegment and inhibits the binding of prorenin to Abs for the anti-handle region (Figure 2A). Moreover, from the studies using Abs to HRP and COS-7 cells expressing rat prorenin receptor protein, we obtained in vitro evidence of prorenin activa-

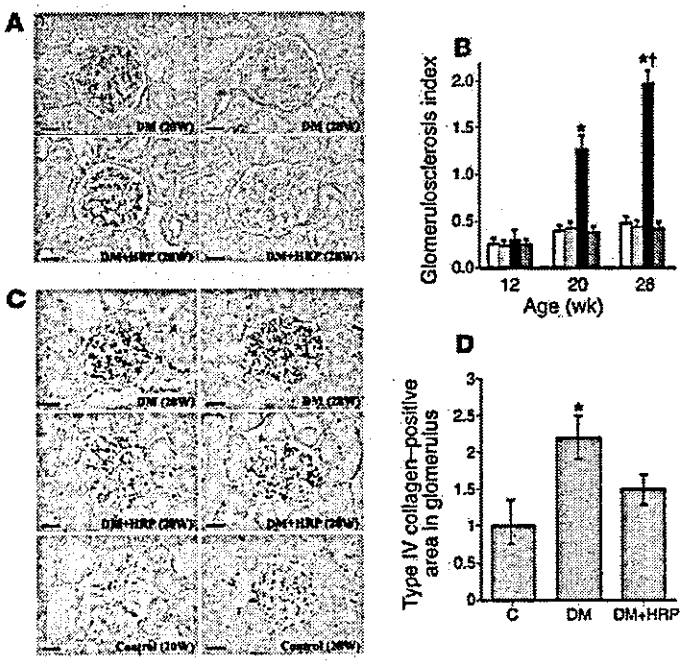

Figure 4
Inhibition of the development of diabetic nephropathy by the HRP of prorenin. (**A**) PAS-stained kidney sections. The photomicrographs show the development and progression of diabetic glomerulosclerosis at 20 weeks of age and later in DM rats. HRP inhibited the development of diabetic glomerulosclerosis in diabetic rats. Scale bars: 50 μm. (**B**) Glomerulosclerosis index of the kidneys in C rats (white bars, $n = 6$), C + HRP rats (light gray bars, $n = 6$), DM rats (black bars, $n = 6$), and DM + HRP rats (dark gray bars, $n = 6$). The graph shows an increase in glomerulosclerosis index at 20 weeks of age and later in DM rats and inhibition of the increase by HRP treatment. $^*P < 0.05$ for DM rats versus the other 3 groups; $^\dagger P < 0.05$ for 28 versus 20 weeks of age. (**C**) Immunohistochemistry of type IV collagen. The photomicrographs show increased glomerular type IV collagen at 20 weeks of age and later in DM rats. HRP inhibited the increase in glomerular type IV collagen in the diabetic rats. Scale bars: 50 μm. (**D**) Quantitative analysis (folds versus C rats) of type IV collagen–positive areas in glomeruli. The graph shows an increase in type IV collagen–positive area in the glomeruli of DM rats at 28 weeks of age and inhibition of the increase by HRP treatment. $^*P < 0.05$ versus C rats.

tion by prorenin receptor or Ab to HRP and inhibition of the activation by HRP. In this mechanism of prorenin activation, we did not see evidence for proteolytic cleavage of prorenin to active renin, suggesting a conformational change as the mechanism. These results support the view that the prorenin elevation in diabetes results in its activation by a nonproteolytic mechanism that is preventable by HRP working as a decoy, which effectively competes for prorenin binding to its receptor inhibiting the proenzyme in activation. Chronic in vivo continuous infusion of HRP by subcutaneous minipumps prevented the increased urinary protein excretion in diabetic rats to levels similar to those of the control rats. HRP did not affect the body weight or blood glucose levels of either control or diabetic rats during 24-week infusion, however, suggesting that HRP did not improve the impaired pancreatic function by the streptozotocin treatment (Figure 3). Also, HRP completely prevented streptozotocin-induced glomerulosclerosis. Also, chronic administration of HRP completely prevented streptozotocin-induced histologically recognizable glomerulosclerosis (Figure 4). These results indicate that the inhibition of nonproteolytic activation of prorenin by HRP completely inhibited the development of nephropathy in rats with streptozotocin-induced diabetes without affecting the hyperglycemic condition.

The ACE inhibitors and Ang II type 1 receptor blockers have significantly attenuated the urinary protein excretion in streptozotocin-induced diabetic rats (10, 11). Prevention of proteinuria and development of glomerulosclerosis in diabetic rats by HRP, however, suggests that HRP may have superior beneficial effects compared with ACE inhibitors or Ang II type 1 receptor blockers. Nguyen et al. recently found that the prorenin/renin receptor(s) is present in the heart, brain, placenta, liver, pancreas, and kidney and activates prorenin by binding proteolysis (9). If HRP competes for prorenin binding to its

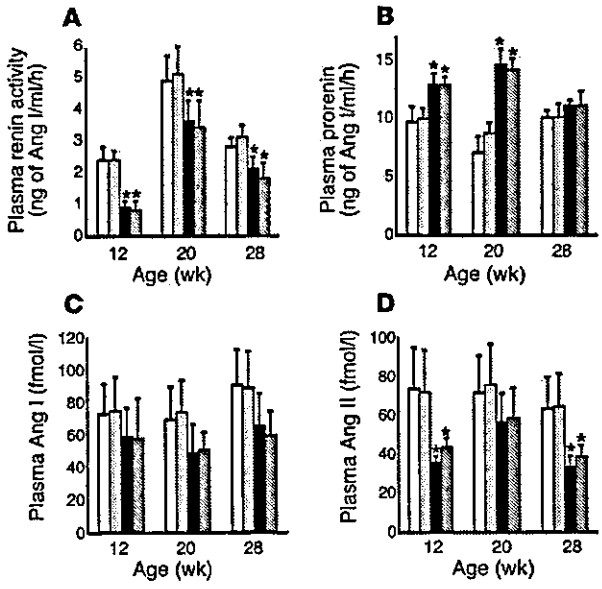

Figure 5
Changes in components of the circulating RAS in C rats (white bars, $n = 6$), C + HRP rats (light gray bars, $n = 6$), DM rats (black bars, $n = 6$), and DM + HRP (dark gray bars, $n = 6$). (**A**) Plasma renin activity. The graph shows decreased plasma renin activity in diabetic rats. HRP did not affect the plasma renin activity of either control or diabetic rats. (**B**) Plasma prorenin concentration. The graph shows increased plasma prorenin concentration in diabetic rats up to 20 weeks of age. HRP did not affect the plasma prorenin concentration of either control or diabetic rats. (**C**) Plasma Ang I concentration. The graph shows a tendency for the plasma Ang I concentration to decrease in diabetic rats. HRP did not affect the plasma Ang I concentration in either control or diabetic rats. (**D**) Plasma Ang II concentration. The graph shows a decreased plasma Ang II concentration in the diabetic rats. HRP did not affect the plasma Ang II concentration in either control or diabetic rats. $^*P < 0.05$ for diabetic versus control rats.

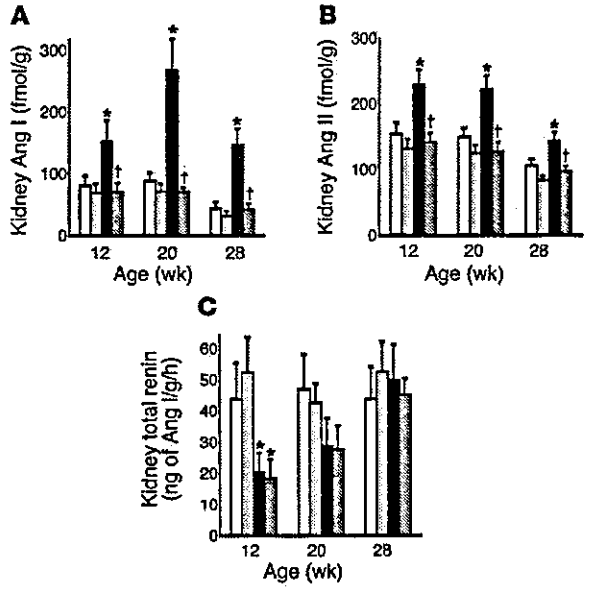

Figure 6
Changes in protein components of the kidney RAS in C rats (white bars, $n = 6$), C + HRP rats (light gray bars, $n = 6$), DM rats (black bars, $n = 6$), and DM + HRP rats (dark gray bars, $n = 6$). (**A**) Kidney Ang I level. The graph shows an increased kidney Ang I level in the DM rats. HRP significantly inhibited the increase in kidney Ang I level in the diabetic rats. (**B**) Kidney Ang II level. The graph shows an increased kidney Ang II level in the DM rats. HRP significantly inhibited the increase in kidney Ang II level in the diabetic rats. (**C**) Kidney total renin level. The graph shows a decreased kidney total renin level in the DM rats at 12 weeks of age. HRP did not affect the kidney total renin level in either control or diabetic rats. $^*P < 0.05$ for DM versus C rats; $^\dagger P < 0.05$ for rats with HRP versus rats without HRP.

receptor resulting in the inhibition of the nonproteolytic activation of prorenin, the complex formation of the prorenin receptor and prorenin may be the major factor in the development of diabetic organ damages. If the complex is also able to activate the ERK1/ERK2 pathways independently of the RAS activation as proposed by Nguyen et al. (9), it is possible that an inhibitor of complex formation between the receptor and prorenin, such as HRP, can completely prevent the development of diabetic organ damages through the inhibition of not only the RAS activation but also the RAS-independent ERK activation.

We measured the RAS components in the plasma of control and diabetic rats (Figure 5). Consistent with previous studies (1, 12), plasma renin activity was significantly lower and plasma prorenin concentration was significantly higher in the DM rats than in the C rats for up to the week 16 of diabetes. The administration of HRP did not affect plasma renin activity or plasma prorenin concentration in either control or the diabetic rats. Although HRP inhibits the interaction between prorenin and its nonproteolytic activators, HRP did not affect the ability of plasma to generate Ang I. The plasma levels of Ang I and II were also lower in the DM rats than in the C rats, and HRP did not influence plasma Ang I or II levels of either control or diabetic rats. In addition, HRP did not affect the BP levels of either control or diabetic rats throughout the 24-week period of HRP infusion. These results suggest that HRP inhibits development of diabetic nephropathy without affecting the circulating RAS or affecting systemic hemodynamics. Since a renin/prorenin receptor, a nonproteolytic activator of prorenin, is exclusively present in tissues but not in circulation (9), HRP may affect tissue RAS but not circulating renin activity or Angs.

There have been conflicting studies showing increased (13), decreased (14), or unchanged (15, 16) kidney Ang II levels in experimental diabetic animals. In these studies, however, kidney Ang II levels were determined at the onset (8 or less weeks) of diabetes without a nephropathy, and to our knowledge, no study had assessed the alterations in the kidney RAS components associated with the development of diabetic nephropathy. In the present study, at 12, 20, and 28 weeks of age (8, 16, and 24 weeks of diabetes), when the diabetic nephropathy developed and progressed, the kidney Ang I and II content of the DM rats markedly increased and was significantly higher than that of the C, C + HRP, and DM + HRP rats (Figure 6, A and B). The kidney Ang I and II content was similar among the C, C + HRP, and DM + HRP rats. The kidney ACE and angiotensinogen mRNA levels were similar in the C, C + HRP, DM, and DM + HRP rats during the 24-week treatment period, consistent with previous studies (17–19) (Figure 7, B and C).

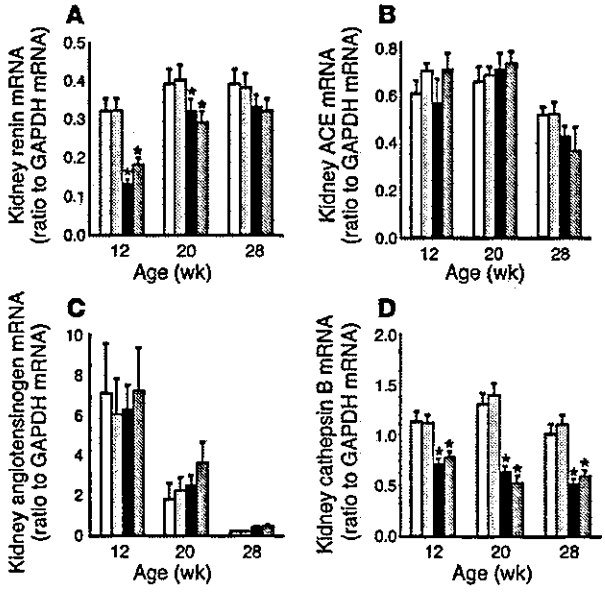

Figure 7
Changes in mRNA components of the kidney RAS in C rats (white bars, $n = 6$), C + HRP rats (light gray bars, $n = 6$), DM rats (black bars, $n = 6$), and DM + HRP rats (dark gray bars, $n = 6$). (**A**) Kidney renin mRNA level. The graph shows a decreased kidney renin mRNA level in the DM rats up to 20 weeks of age. HRP did not affect the kidney renin mRNA level in either control or diabetic rats. (**B**) Kidney ACE mRNA level. The graph shows a decrease in kidney ACE mRNA level at 28 weeks of age in both the control and diabetic rats. HRP did not affect the kidney ACE mRNA level in either control or diabetic rats. (**C**) Kidney angiotensinogen mRNA level. The graph shows a decrease in kidney angiotensinogen mRNA level with age. HRP did not affect the kidney angiotensinogen mRNA level in either control or diabetic rats. (**D**) Kidney cathepsin B mRNA level. The graph shows a decreased kidney cathepsin B mRNA level in the DM rats. HRP did not affect the kidney cathepsin B mRNA level in either control or diabetic rats. $^*P < 0.05$ for diabetic versus control rats.

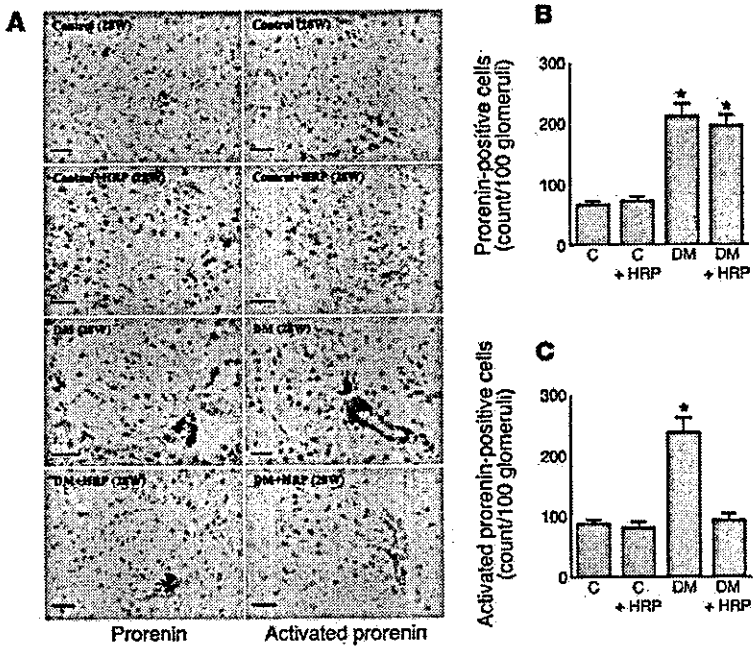

Figure 8
Kidney levels of total prorenin and activated prorenin in C rats ($n = 6$), C + HRP rats ($n = 6$), DM rats ($n = 6$), and DM + HRP rats ($n = 6$) at 28 weeks of age. **(A)** Immunohistochemistry of prorenin and active center of renin that indicates total prorenin and activated prorenin, respectively. The photomicrographs show increases in both total prorenin and activated prorenin at the juxtaglomerular area of diabetic rat kidneys. HRP treatment did not alter the increased staining of total prorenin but inhibited the enhanced staining of activated prorenin. Scale bars: 25 μm. **(B)** Quantitative analysis of prorenin-positive cells in a juxtaglomerular area. The graph shows an increase in prorenin-positive cells in DM and DM + HRP rats. **(C)** Quantitative analysis of activated prorenin in a juxtaglomerular area. The graph shows an increase in activated prorenin in DM and its inhibition by HRP treatment. $^*P < 0.05$ versus C rats.

However, since high extracellular glucose stimulates the synthesis of angiotensinogen in a concentration-dependent manner in rat proximal tubular cells (20), the present study cannot exclude the possibility that angiotensinogen synthesis regionally increases in the proximal tubule (13, 21) or even in the glomerulus. Previous studies showed that kidney renin mRNA levels increased at the early onset of diabetes in spontaneously or streptozotocin-induced diabetic rats (13, 17, 19, 21) and decreased markedly thereafter (17). The present study demonstrated that both the total kidney renin (proteolytically activated and prorenin) content and kidney renin mRNA level were lower in the DM rats than in the C rats at 12 and 20 weeks of age (8 and 16 weeks of diabetes) when the nephropathy develops, and they were similar at 28 weeks of age (24 weeks of diabetes) when the nephropathy progresses. HRP administration did not alter total kidney renin content or kidney renin mRNA levels in either control or diabetic rats at any age or length of diabetes (Figure 6C and 7A). Thus, the total amount of intrarenal renin and prorenin generated in the kidneys may be decreased during the development of diabetic nephropathy. The total activity of renin and prorenin did increase in the kidneys of diabetic rats, however, because the result of the present study showed the increased staining of the exposed active center of renin/prorenin in the kidneys of diabetic rats and its inhibition by HRP. Previous studies also demonstrated increased ability of the kidney to generate Ang I in diabetic rats, which was called "renal renin concentration" (21). Taken together, during the development of diabetic nephropathy, the kidneys of diabetic rats increased levels of Ang I and II without any changes in renin, ACE, or angiotensinogen synthesis, and continuous infusion of HRP completely inhibited the increased kidney levels of Ang I and II without affecting the kidney levels of renin, ACE, or angiotensinogen mRNA. These results suggest that intrarenal renin activity increases during the development of diabetic nephropathy and that nonproteolytic activation of prorenin significantly contributes to the increased intrarenal renin activity.

The reason why the nonproteolytic activation of prorenin occurs in diabetic organ remains unclear. We believe, however, that the present studies provide a credible explanation. Consistent with previous in vitro and in vivo studies (22, 23), the kidney cathepsin B mRNA levels significantly decreased during the development of diabetic nephropathy (Figure 7D). This result suggests that the decreased prorenin processing can increase the ratio of prorenin to renin in diabetic rat kidneys. In fact, the immunohistochemical staining of prorenin significantly increased in diabetic rat kidneys compared with control rat kidneys (Figure 8, A and B), although total renin content of diabetic rat kidneys was similar to or lower than that of control rat kidneys (Figure 6C). Since both renin and prorenin competitively bind to a renin/prorenin receptor (9), the relative increase in prorenin versus renin could cause more binding of prorenin to its receptor, leading to the nonproteolytic activation of prorenin. This idea was supported by the result of the present study showing that the inhibition of nonproteolytic activation of prorenin by HRP significantly suppresses the increased immunohistochemical staining of exposed active center of renin/prorenin in the kidneys of diabetic rats (Figure 8, A and C). Alternatively, nonproteolytic prorenin-activators, such as a renin/prorenin receptor (9), or their affinity to prorenin might be increased in diabetic organ. Further studies will be needed to determine the reason why the nonproteolytic activation of prorenin occurs in the diabetic organ.

In conclusion, even though diabetic animals have high plasma prorenin levels and low plasma renin levels, suggesting a suppressed circulating RAS (1), Ang II type 1 receptor blockers have a beneficial effect in preventing the development and progression of diabetic organ damage (24, 25). This study clearly demonstrated that the development of diabetic nephropathy is associated with the activated kidney RAS and suggested that nonproteolytic activation of prorenin significantly contributes to the activation of the kidney RAS and the development of diabetic nephropathy.

Therefore, we propose that substances that inhibit nonproteolytic activation of prorenin, such as HRP, is useful in drug therapy strategies to prevent diabetic organ damage.

Methods

Preparation of rat prorenin handle peptide and its Ab. Figure 1 shows the prosegment of rat prorenin. To cover the handle region (position 11–15) (5), we designed a decapeptide, NH_2-RILLKKMPSV-COOH, as an HRP of rat prorenin and purified it by HPLC on a C-18 reverse-phase column. The purity and retention time of HPLC were 97.6% and 26.2 minutes, respectively. The mass of the product was 1,185.7, similar to the theoretical mass value (1,186.0). Anti-rat HRP Ab was raised against a peptide, RILLKK-MPSVC, conjugated with keyhole limpet hemocyanin in rabbits. HRP was used for determining the titer of the antiserum using a Vectastatin ABC-AP rabbit IgG kit (Vector Laboratories) and as the ligand of an affinity column for purification of the Ab. High-titer antisera were obtained 6 weeks after the first immunization. The affinity gel was prepared by conjugation of Biogel 102 (amine-coupled gel; Bio-Rad Laboratories) through a cysteine residue of antigen peptide as a ligand. The Ab was purified with the affinity column, and the concentration of the purified Ab (3.90 mg/ml) was calculated using an extinction coefficient of 1.35 at 1 mg/ml IgG and 280 nm.

Immunoblot analysis. The recombinant rat prorenin and renin was subjected to 12% SDS-PAGE and electrophoretically transferred to the polyvinylidene difluoride membrane. Renin was prepared by the trypsin treatment of prorenin; that is, prorenin was incubated with 200 μg/ml of trypsin for 20 minutes at pH 7.4 and 25°C, and then the trypsin action was arrested with 1 mM PMSF. The membrane was incubated separately with rabbit anti-rat renin antiserum (1:1,000) (26) and 3 nM purified rabbit anti-handle region peptide Ab for 1 hour at room temperature in the absence or presence of 10, 100, and 1,000 nM regional peptides of prorenin prosegment. After being washed, the immunocomplex on these sheets was visualized using horseradish peroxidase–conjugated secondary anti-rabbit IgG and diaminobenzidine.

Animals. We maintained male Sprague-Dawley rats (Charles River Laboratories Inc.) in a temperature-controlled room that was maintained at 23°C and a 12-hour light/12-hour dark cycle, with free access to water and a normal-salt diet rat chow (0.4% NaCl) (CE-2; Nihon Clea). The Keio University Animal Care and Use Committee approved all experimental protocols. At 3 weeks of age, under sodium pentobarbital (50 mg/kg i.p.) anesthesia, we removed the left kidney of 100- to 150-g rats and divided the heminephrectomized rats into four groups: the C, C + HRP, DM, and DM + HRP groups. Diabetic rats received i.p. 10 mM citrate buffer with 65 mg/kg of streptozotocin (Wako Pure Chemical), and nondiabetic control rats received 10 mM citrate buffer alone, at 4 weeks of age. Every 28 days we changed the subcutaneously implanted osmotic minipump (model 2004, for 28-day use; Alzet Osmotic Pumps) containing saline or a HRP (0.1 mg/kg), and we decapitated six rats at 12, 20, and 28 weeks of age to obtain the blood and right kidney of each animal. In our preliminary study, an osmotic minipump with a NH_2-SFGR-COOH (0.1 mg/kg, $n = 3$) or NH_2-MTRI-SAE-COOH (0.1 mg/kg, $n = 3$) was also implanted in diabetic rats. These peptides, however, did not inhibit the development of glomerulosclerosis or increase in the levels of Ang I and II in the kidneys of diabetic rats.

Experiments. We measured the systolic arterial BP of the rats at 4, 8, 12, 16, 20, 24, and 28 weeks of age by tail-cuff plethysmography. The 24-hour urine was collected in a metabolic cage, and urinary protein excretion and creatinine were determined with a Micro TP test kit (Wako Pure Chemical) and a creatinine HA test kit (Wako Pure Chemical), respectively. Blood was obtained from the tail vein, and glucose was analyzed with a glucose C test kit (Wako Pure Chemical).

Morphological and immunohistochemical evaluation. A part of the kidney removed from each animal was fixed in 10% formalin in phosphate buffer (pH 7.4). Paraffin-embedded sections were stained by the PAS method. We quantitatively determined the total area of sclerosis within the glomerular tuft, adopting the semiquantitative scoring system proposed by El-Nahas, et al. (27). A glomerulosclerosis index was derived for each animal by examining 100 glomeruli at ×400 magnification. The severity of glomerulosclerosis was expressed on an arbitrary scale from 0 to 4: grade 0, normal glomeruli; grade 1, presence of mesangial expansion/thickening of the basement membrane; grade 2, mild to moderate segmental hyalinosis/sclerosis involving less than 50% of the glomerular tuft; grade 3, diffuse glomerular hyalinosis/sclerosis involving more than 50% of the tuft; grade 4, diffuse glomerulosclerosis with total tuft obliteration and collapse. The resulting index in each animal was expressed as a mean of all scores obtained.

For immunohistochemical staining, deparaffinized sections were pretreated with proteinase K, the sections were then boiled in citrate buffer with microwaves to unmask antigenic sites, and endogenous biotin was blocked with a biotin-blocking system (X0590; DAKO Corp.). Next, the sections were immersed in 3% H_2O_2 in methanol to inhibit endogenous peroxidase and then precoated with 1% nonfat milk in PBS to block nonspecific binding. For immunohistochemical staining of type IV collagen and prorenin, a cocktail of rabbit polyclonal Abs to the anti-a2(IV), -a4(IV), and -a5(IV) chains of type IV collagen (1:400; a generous gift of R. Kalluri, Center for Matrix Biology, Beth Israel Deaconess Medical Center) (28) and the rabbit anti-rat HRP Ab were applied, respectively, to the sections as the primary Ab. The sections were incubated with a biotin-conjugated anti-rabbit IgG as the secondary Ab. For immunohistochemical staining of the exposed active center of renin, a goat polyclonal Ab to rat renin that crossreacts with nonproteolytically activated prorenin but not with natural prorenin (1:1,000) (26, 29, 30) was applied to the sections as the primary Ab. The sections were incubated with a biotin-conjugated anti-goat IgG as the secondary Ab. The Ab reactions were visualized by using a VectaStain ABC Standard Kit (Vector Laboratories) and an AEC standard kit (DAKO Corp.) according to the manufacturers' instructions. We quantitatively determined the immunoreactive type IV collagen-positive area in each glomerulus at ×200 magnification with a Mac SCOPE (version 2.5; Mitani Corp.) and expressed it as a percentage of the whole cross-sectional area of the glomerulus. The levels of prorenin and the exposed active center of renin were evaluated by counting the number of juxtaglomerular cells where the signal intensity of the reaction products was above the visible level. The final overall score was calculated as the means of the values for 100 glomeruli per group of rats.

Measurements of renin and Ang peptides. Immediately after decapitation, a 3-ml blood specimen was collected into a tube containing 30 μl of EDTA (500 mM), 15 μl of enalaprilat (1 mM), and 30 μl of *o*-phenanthroline (24.8 mg/ml) and pepstatin (0.2 mM), and plasma samples were obtained by centrifugation. Plasma renin activity was determined with a RIA coated bead kit (Dinabott Radioisotope Institute). Plasma prorenin level was calculated by subtracting plasma renin activity from plasma total (inactive plus active) renin activity, as described previously (31). For the measurement of kidney total renin content, a part of the removed kidney was weighed, placed in 5 ml of buffer containing 2.6 mM EDTA, 1.6 mM dimercaprol, 3.4 mM 8-hydroxyquinoline sulfate, 0.2 mM PMSF, and 5 mM ammonium acetate, homogenized with a chilled glass homogenizer, and then centrifuged. The renin activity of the supernatant was determined as described previously (32). For the determination of kidney Ang I and II content, half of the removed kidney was weighed, placed in ice-cold methanol (10% wt/vol), homogenized with a chilled glass homogenizer, and then centrifuged. The supernatant was then dried and reconstituted in 4 ml of 50 mM sodium phosphate buffer containing 1% albumin. Plasma and reconstituted samples from the kidneys were extracted with a Bond-Elut column (Analytichem Co.), and the eluents were evaporated to dryness and reconstituted in Ang peptide assay diluent. The Ang I and II content was quantitatively